Simultaneous formation of helical and sheet-like assemblies from short azapeptides enables spontaneous resolution

Xiaosheng Yan,*[a,b] Peimin Weng,[a] Jinlian Cao,[a] Kexin Lin,[b] Yuanwei Qi,[b] Xin Wu,[b] and Yun-Bao Jiang*[a]

[a] Department of Chemistry, College of Chemistry and Chemical Engineering, The MOE Key Laboratory of Spectrochemical Analysis and Instrumentation, and *i*ChEM, Xiamen University, Xiamen 361005, China.

[b] Fujian Provincial Key Laboratory of Innovative Drug Target Research and State Key Laboratory of Cellular Stress Biology, School of Pharmaceutical Sciences, Xiamen University, Xiamen, Fujian 361102, China.

*E-mail: xshyan@xmu.edu.cn; ybjiang@xmu.edu.cn.

Supporting Information

Contents

1. Syntheses and characterizations

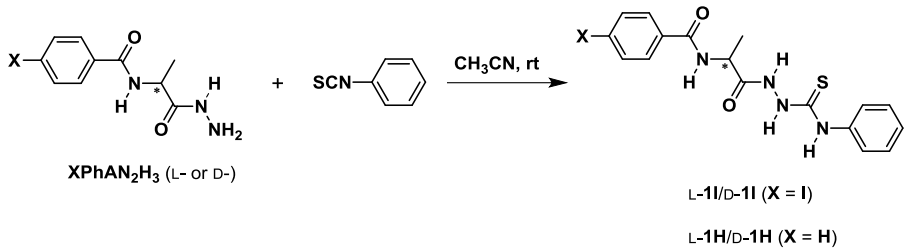

Scheme S1. General procedures for the syntheses of **1I** and **1H**

Compounds **$XPhAN_2H_3$** (**X** = **I**, **H**) were synthesized according to the same procedure as that reported in the literature.[S1]

1I: To a CH_3CN solution (20 mL) of **$IPhAN_2H_3$** (0.50 g, 1.50 mmol), excess phenyl isocyanate (0.5 mL) was added, and the mixture was stirred for 24 h at room temperature. After filtration, the solid was recrystallized in CH_3CN and dried in vacuum to obtain **1I** (0.60 g, 85% yield).

1H: To a CH_3CN solution (20 mL) of **$HPhAN_2H_3$** (0.40 g, 1.93 mmol), excess phenyl isocyanate (0.6 mL) was added, and the mixture was stirred for 24 h at room temperature. After concentration in vacuum, the solid was washed by Et_2O, and then recrystallized in CH_3CN and dried in vacuum to obtain **1H** (0.50 g, yield 75%).

L-**1I**: ^{1}H NMR (500 MHz, DMSO-d_6): δ (ppm) 10.38 (s, 1H), 9.72 (s, 1H), 9.25 (s, 1H), 8.97 (s, 1H), 7.89 (d, J = 8.3 Hz, 2H), 7.66 (dd, J = 16.5, 7.5 Hz, 4H), 7.35 (t, J = 7.8 Hz, 2H), 7.16 (t, J = 7.3 Hz, 1H), 4.32 (s, 1H), 1.40 (d, J = 7.0 Hz, 3H); ^{13}C NMR (151 MHz, DMSO-d_6): δ (ppm) 180.13, 171.76, 166.85, 139.00, 137.17, 132.75, 129.56, 128.15, 124.82, 124.09, 99.50, 49.17, 16.54; HRMS (ESI): calcd for $[C_{17}H_{17}IN_4NaO_2S]^+$: 491.0015, found: 491.0005.

D-**1I**: ^{1}H NMR (500 MHz, DMSO-d_6): δ (ppm) 10.38 (s, 1H), 9.71 (s, 1H), 9.26 (s, 1H), 8.98 (s, 1H), 7.89 (d, J = 7.2 Hz, 2H), 7.76 – 7.53 (m, 4H), 7.42 – 7.28 (m, 2H), 7.20 – 7.11 (m, 1H), 4.33 (s, 1H), 1.39 (d, J = 6.3 Hz, 3H); ^{13}C NMR (151 MHz, DMSO-d_6): δ (ppm) 180.16, 171.77, 166.85, 139.01, 137.17, 132.75, 129.56, 128.15, 124.83, 124.10, 99.50, 49.15, 16.56; HRMS (ESI): calcd for $[C_{17}H_{17}IN_4NaO_2S]^+$: 491.0015, found: 491.0007.

L-**1H**: ^{1}H NMR (500 MHz, DMSO-d_6): δ (ppm) δ 10.41 (s, 1H), 9.72 (s, 1H), 9.31 (s, 1H), 8.92 (s, 1H), 7.90 (d, J = 7.5 Hz, 2H), 7.68 (d, J = 5.6 Hz, 2H), 7.56 (t, J = 7.3 Hz, 1H), 7.49 (t, J = 7.5 Hz, 2H), 7.35 (t, J = 7.7 Hz, 2H), 7.16 (t, J = 7.1 Hz, 1H), 4.32 (s, 1H), 1.41 (d, J = 7.0 Hz, 3H); ^{13}C NMR (214 MHz, CD_3CN): δ (ppm) 182.78, 173.06, 169.63, 139.81, 134.12, 133.05, 129.51,

129.34, 128.45, 126.59, 125.61, 51.15, 16.76; HRMS (ESI): calcd for $[C_{17}H_{18}N_4NaO_2S]^+$: 365.1048, found: 365.1043.

D-**1H**: ^{1}H NMR (500 MHz, DMSO-d_6): δ (ppm) 10.40 (s, 1H), 9.72 (s, 1H), 9.31 (s, 1H), 8.92 (s, 1H), 7.90 (d, J = 7.8 Hz, 2H), 7.68 (d, J = 6.0 Hz, 2H), 7.56 (t, J = 7.3 Hz, 1H), 7.48 (t, J = 7.5 Hz, 2H), 7.35 (t, J = 7.6 Hz, 2H), 7.16 (t, J = 6.8 Hz, 1H), 4.33 (s, 1H), 1.41 (d, J = 7.1 Hz, 3H); ^{13}C NMR (214 MHz, CD_3CN): δ (ppm) 182.79, 173.06, 169.63, 139.81, 134.13, 133.06, 129.51, 129.34, 128.45, 126.59, 125.61, 51.16, 16.76; HRMS (ESI): calcd for $[C_{17}H_{18}N_4NaO_2S]^+$: 365.1048, found: 365.1040.

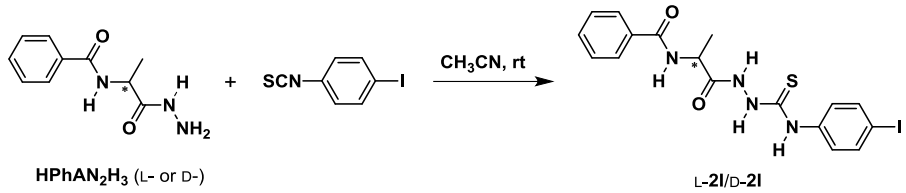

Scheme S2. General procedures for the syntheses of **2I**

2I: To a CH_3CN solution (20 mL) of **$HPhAN_2H_3$** (0.40 g, 1.93 mmol), 4-iodophenyl isocyanate (0.55 g, 2.11 mmol) was added, and the mixture was stirred for 24 h at room temperature. After concentration in vacuum, the solid was washed by Et_2O, and then recrystallized in CH_3CN and dried in vacuum to obtain **2I** (0.71 g, yield 79%).

L-**2I**: ^{1}H NMR (500 MHz, DMSO-d_6): δ (ppm) 10.43 (s, 1H), 9.85 (s, 1H), 9.33 (s, 1H), 8.95 (s, 1H), 7.91 (d, J = 7.4 Hz, 2H), 7.70 (d, J = 8.3 Hz, 2H), 7.65 – 7.52 (m, 3H), 7.50 (t, J = 7.5 Hz, 2H), 4.30 (s, 1H), 1.41 (d, J = 6.9 Hz, 3H); ^{13}C NMR (214 MHz, DMSO-d_6): δ (ppm) 179.99, 171.92, 167.68, 138.99, 136.82, 133.18, 131.77, 128.31, 127.65, 126.01, 89.18, 49.25, 16.48; HRMS (ESI): calcd for $[C_{17}H_{17}IN_4NaO_2S]^+$: 491.0015, found: 491.0012.

D-**2I**: ^{1}H NMR (500 MHz, DMSO-d_6): δ (ppm) 10.43 (s, 1H), 9.84 (s, 1H), 9.33 (s, 1H), 8.95 (s, 1H), 7.91 (d, J = 7.4 Hz, 2H), 7.70 (d, J = 8.2 Hz, 2H), 7.66 – 7.52 (m, 3H), 7.49 (t, J = 7.4 Hz, 2H), 4.31 (s, 1H), 1.41 (d, J = 6.8 Hz, 3H); ^{13}C NMR (214 MHz, DMSO-d_6): δ (ppm) 180.02, 171.97, 167.73, 139.01, 136.85, 133.18, 131.79, 128.33, 127.67, 126.05, 89.21, 49.31, 16.51; HRMS (ESI): calcd for $[C_{17}H_{17}IN_4NaO_2S]^+$: 491.0015, found: 491.0013.

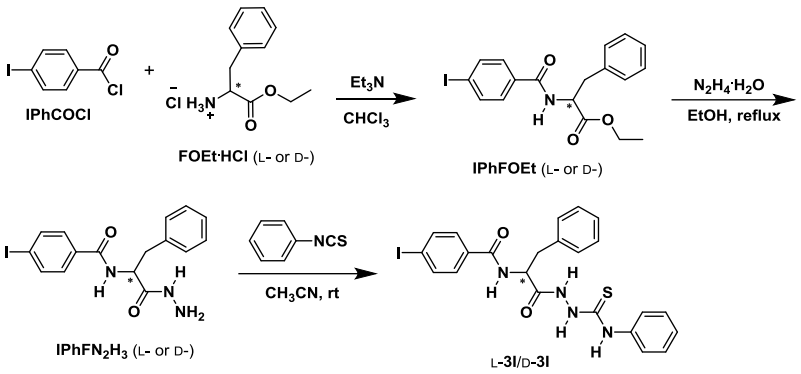

Scheme S3. General procedures for the syntheses of **3I**

3I: To a $CHCl_3$ solution (40 mL) of ethyl phenylalaninate hydrochloride (**FOEt·HCl**, L- or D-, 2.30 g, 10.0 mmol) and Et_3N (3.0 mL), 4-iodobenzoyl chloride (**IPhCOCl**, 2.93 g, 11.0 mmol) was added, and the mixture was stirred for 12 h at room temperature. The solvent was removed by evaporated in vacuo. The solid residue was dissolved in EtOAc and then the solution was washed successively with 1% $NH_3·H_2O$, 1% HCl and saturated NaCl solutions. The solution was then dried over anhydrous Na_2SO_4 and concentrated in vacuo, generating solid product **IPhFOEt** (3.46 g, yield 82%). Excess aqueous hydrazine (85%, 6.0 mL) was added to **IPhFOEt** in EtOH (40 mL) and the mixture was refluxed for 24 hours. The solvent was removed by evaporated in vacuo, and the crude product was washed with CH_3CN several times to afford white solid product **IPhFN$_2$H$_3$** (2.85g, yield 85%). To a CH_3CN solution (30 mL) of **IPhFN$_2$H$_3$** (0.50 g, 1.22 mmol), excess phenyl isocyanate (0.5 mL) was added, and the mixture was stirred for 24 h at room temperature. After filtration, the solid was washed by CH_3CN and Et_2O, and then dried in vacuum to obtain **3I** (0.57 g, yield 86%).

L-**3I**: ^{1}H NMR (500 MHz, DMSO-d_6): δ (ppm) 10.44 (s, 1H), 9.77 (s, 1H), 9.21 (s, 1H), 8.94 (s, 1H), 7.85 (d, J = 8.2 Hz, 2H), 7.58 (t, J = 7.2 Hz, 4H), 7.34 (dd, J = 13.3, 5.6 Hz, 4H), 7.27 (t, J = 7.5 Hz, 2H), 7.17 (dd, J = 16.1, 7.5 Hz, 2H), 4.60 (s, 1H), 3.23 (s, 1H), 3.14 – 3.02 (m, 1H); ^{13}C NMR (151 MHz, DMSO-d_6): δ (ppm) 180.26, 170.78, 166.84, 139.01, 137.83, 137.20, 132.97, 129.48, 129.24, 128.25, 126.44, 125.03, 124.58, 99.48, 54.62, 36.03; HRMS (ESI): calcd for $[C_{23}H_{21}IN_4NaO_2S]^+$: 567.0328, found: 567.0327.

D-**3I**: ^{1}H NMR (500 MHz, DMSO-d_6): δ (ppm) 10.45 (s, 1H), 9.79 (s, 1H), 9.21 (s, 1H), 8.97 (s, 1H), 7.86 (d, J = 8.2 Hz, 2H), 7.57 (t, J = 6.9 Hz, 4H), 7.34 (dd, J = 15.8, 7.9 Hz, 4H), 7.27 (t, J = 7.6 Hz, 2H), 7.18 (dd, J = 16.8, 7.8 Hz, 2H), 4.58 (s, 1H), 3.22 (s, 1H), 3.11 – 3.02 (m, 1H); ^{13}C NMR (126 MHz, DMSO-d_6): δ (ppm) 180.39, 170.69, 166.69, 138.98, 137.80, 137.14, 132.97, 129.42, 129.18, 128.19, 126.38, 124.91, 124.40, 99.33, 54.47, 36.07; HRMS (ESI): calcd for $[C_{23}H_{21}IN_4NaO_2S]^+$: 567.0328, found: 567.0323.

2. Experimental data

Table S1. Crystallographic data for L-**1I** and D-**1I**

Compound reference	L-**1I** [a]	D-**1I** [a]
Empirical formula	$C_{17}H_{17}IN_4O_2S$	$C_{17}H_{17}IN_4O_2S$
Formula weight	468.30	468.30
Temperature/K	100.1(2)	99.9(7)
Crystal system	orthorhombic	orthorhombic
Space group	$P2_12_12_1$	$P2_12_12_1$
a/Å	4.65650(10)	4.65680(10)
b/Å	16.8753(3)	16.8731(4)
c/Å	22.9925(4)	22.9659(6)
α/°	90	90
β/°	90	90
γ/°	90	90
Volume/Å^3	1806.75(6)	1804.54(7)
Z	4	4
ρ_{calc}g/cm^3	1.722	1.724
μ/mm^{-1}	15.167	15.186
F(000)	928.0	928.0
Crystal size/mm^3	0.42 × 0.26 × 0.22	0.26 × 0.24 × 0.16
Radiation	CuKα (λ = 1.54184)	CuKα (λ = 1.54184)
2Θ range for data collection/°	6.498 to 121.986	6.5 to 153.93
Index ranges	-5 ≤ h ≤ 3, -19 ≤ k ≤ 19, -25 ≤ l ≤ 26	-5 ≤ h ≤ 5, -19 ≤ k ≤ 21, -26 ≤ l ≤ 27
Reflections collected	5001	6214
Independent reflections	2638 [R_{int} = 0.0522, R_{sigma} = 0.0627]	3149 [R_{int} = 0.0528, R_{sigma} = 0.0616]
Data/restraints/parameters	2638/150/227	3149/0/227
Goodness-of-fit on F^2	1.156	1.145
Final R indexes [I>=2σ (I)]	R_1 = 0.0585, wR_2 = 0.1556	R_1 = 0.0377, wR_2 = 0.0930
Final R indexes [all data]	R_1 = 0.0615, wR_2 = 0.1741	R_1 = 0.0449, wR_2 = 0.1190
Largest diff. peak/hole / e Å^{-3}	1.36/-1.41	1.67/-1.11
Flack parameter	-0.007(11)	-0.013(7)
CCDC number	1998162	1998163

[a] Grown in *i*PrOH solution via slow evaporation.

Table S2. Torsions, types of β-turns and geometrical parameters and calculated interaction energies of intramolecular ten-membered ring hydrogen bonds revealed by the X-ray crystal structures

Crystal structure	L-**1I**	D-**1I**	L-**1H**	D-**1H**	*rac*-**1H**@L-**1H**	*rac*-**1H**@D-**1H**
φ_{i+1} / º	-58.77	57.81	-55.64	55.85	60.58	60.58
ψ_{i+1} / º	135.97	-136.46	141.58	-141.66	134.91	-134.91
φ_{i+2} / º	70.72	-69.07	67.56	-67.90	76.33	-76.33
ψ_{i+2} / º	8.37	-9.99	14.98	-14.86	2.08	-2.08
Type[S2]	II	II’	II	II’	II	II’
Length [a] / Å	2.117	2.147	2.392	2.387	2.109	2.109
Angle [b] / º	149.40	147.96	137.94	137.89	148.90	148.90
E_{nb} [c] / kJ mol^{-1}	-11.8	-10.9	-5.76	-5.85	-12.7	-11.8

[a] Distance of $H^{d}\cdots O^{e}$. [b] Angle of $NH^{d}O^{e}$. Labels of atoms are shown in Figure 2a. [c] Interaction energy of intramolecular $N-H^{d}\cdots{}^{e}O=C$ hydrogen bond analyzed by Quantum Theory of Atoms In Molecules (QTAIM). Method: B3LYP DFT with the 6-311G** basis set for C, H, O, N, S, and LANL2DZ for I atoms, POP=NBO.

Table S3. Geometrical parameters and calculated interaction energies of intermolecular interactions revealed by the X-ray crystal structures

Crystal	Interaction	Length / Å	Angle / º	ΔE [c] / kJ mol^{-1}
L-**1I**	$N-H^{b}\cdots{}^{f}O=C$	2.034	157.77 (∠NHO) 150.49 (∠HOC)	-107.5
	C−I···π	3.896 [a]	163.67 [b]	-31.59
	$N-H^{a}\cdots S=C$	2.623	163.65 (∠NHS) 124.08 (∠HSC)	-63.30
L-**1H**	$N-H^{b}\cdots{}^{f}O=C$	2.113	152.71 (∠NHO) 151.27 (∠HOC)	-103.59
	$N-H^{a}\cdots S=C$	2.669	153.67 (∠NHS) 118.10 (∠HSC)	-53.24
rac-**1H**	$N-H^{a}\cdots{}^{f}O=C$	2.264	150.67 (∠NHO) 157.93 (∠HOC)	-60.91
	$N-H^{c}\cdots S=C$	2.471	167.44 (∠NHS) 112.02 (∠HSC)	-50.48 [d]
	$N-H^{b}\cdots{}^{i}O-H^{h}$	1.977	175.67 (∠NHO) 109.57 (∠HOC)	-26.05
	$^{i}O-H^{h}\cdots S=C$	2.468	145.91 (∠OHS) 126.97 (∠HSC)	-18.84

[a] Distance of iodine to the centroid of benzene ring. [b] Angle of C, I and the centroid of benzene ring. [c] Method: WB97XD DFT with the 6-31+G(d,p) basis set for C, H, O, N, S, and LANL2DZ for I atoms. [d] Interaction energy of double $N-H^{c}\cdots S=C$ hydrogen bonds.

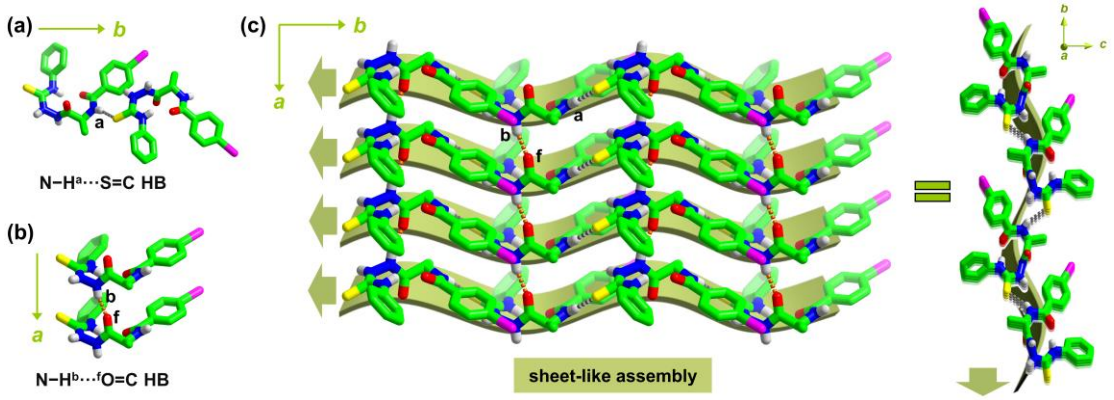

Figure S1. (a) Intermolecular N−H^{a}···S=C hydrogen bond (HB, dashed gray line) along *b*-axis of L-**1I** crystal. (b) Intermolecular N−H^{b}···^{f}O=C hydrogen bond (HB, dashed orange line) along *a*-axis of L-**1I** crystal. (c) Sheet-like 2D assembly from L-**1I** within *ab* plane, supported by N−H^{a}···S=C hydrogen bonds (dashed gray lines) along *b*-axis and N−H^{b}···^{f}O=C hydrogen bonds (dashed orange lines) along *a*-axis. For clarity, −CH protons are omitted. The thick arrows indicate the direction of *N*- to *C*-terminus of L-**1I** along the strand structure.

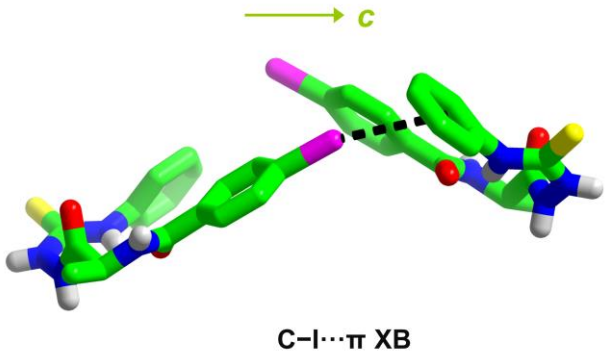

Figure S2. Intermolecular C−I···π halogen bond (XB, dashed black line) along *c*-axis of L-**1I** crystal. For clarity, −CH protons are omitted.

Table S4. Natural bond orbital (NBO) analysis[a] for intermolecular C−I···π interaction in L-**1I** dimer

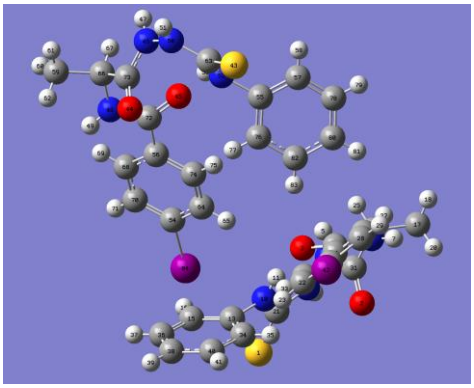

Interaction	Donor	Acceptor	$E^{(2)}$ (kJ mol^{-1})[b]
C−I···π	BD(2)(C^{36}–C^{38})	σ*(I^{84}–C^{54})	1.13
	BD(1)(C^{38}–C^{40})		0.25
	LP(1)(C^{40})		9.24

[a] Method: WB97XD DFT with the 6-31+G(d,p) basis set for C, H, O, N, S, and LANL2DZ for I atoms. POP = NBO. [b] The second-order perturbation energy.

Table S5. Topological parameters (ρ and $\nabla^2\rho$) of the intermolecular critical point 29 in L-**1I** dimer for C−I···π halogen bond and the calculated interaction energy (E_{nb}) analyzed by Quantum Theory of Atoms In Molecules (QTAIM)

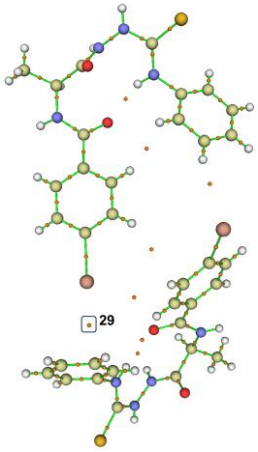

Critical point	Contact	ρ	$\nabla^2\rho$	E_{nb} (kJ mol^{-1})
29	C−I···π	0.008	0.025	-6.76

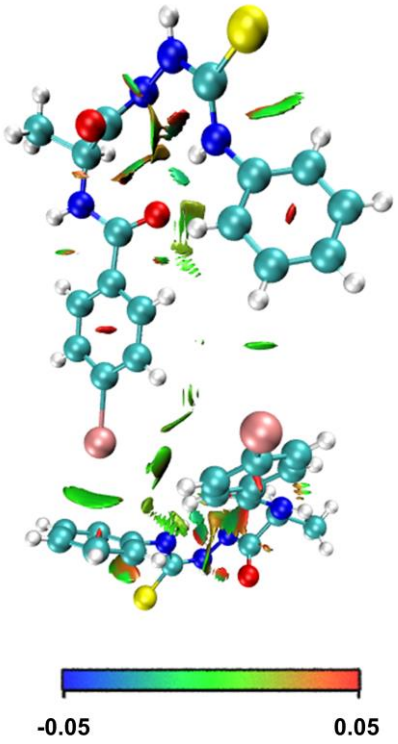

Figure S3. Noncovalent interaction (NCI) surfaces (-0.05 to 0.05 a.u.) for representative C−I···π halogen bond in L-**1I** dimer. Color code: red for repulsive, yellow for weakly repulsive, green for weakly attractive, and blue for strongly attractive forces.

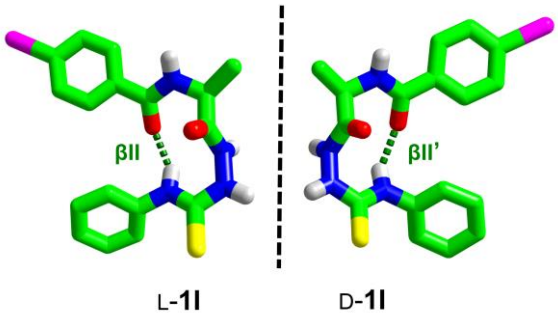

Figure S4. Crystal structures of L-**1I** and D-**1I**, showing βII and βII'-turns, respectively. For clarity, −CH protons are omitted.

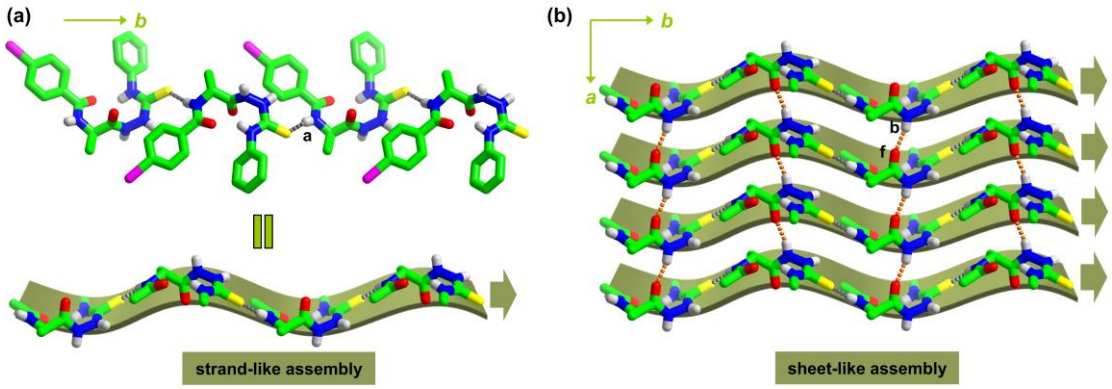

Figure S5. (a) Strand-like 1D assembly from D-**1I** molecules along *b*-axis via intermolecular N−H^{a}···S=C hydrogen bonds (dashed gray lines). (b) N−H^{b}···^{f}O=C hydrogen bonds (dashed orange lines) along *a*-axis link parallel strand-like 1D assemblies into a sheet-like 2D assembly within *ab* plane. For clarity, −CH protons are omitted, in the strand and sheet-like assemblies, iodophenyl and phenyl rings are also omitted. The thick arrows indicate the direction of *N*- to *C*-terminus of D-**1I** along the strand structure.

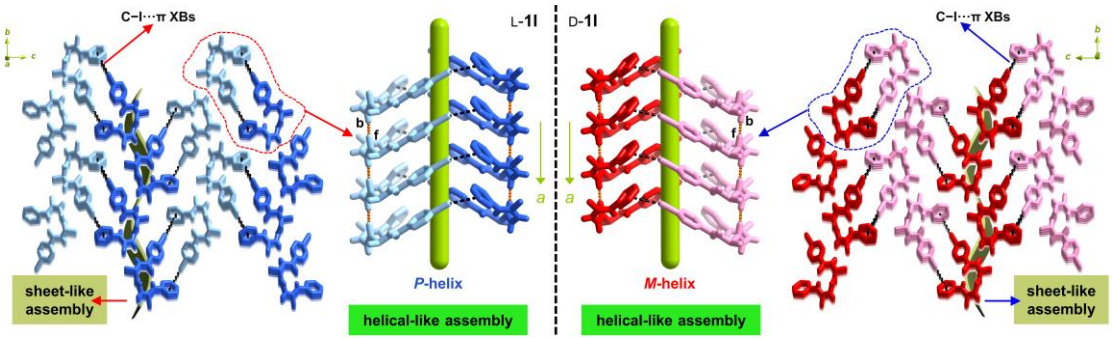

Figure S6. Mirror symmetric 3D superstructures from L-**1I** (left) and D-**1I** (right), consisting of helical and sheet-like assemblies. While *P*-helix is formed in L-**1I** crystal, *M*-helix is formed in D-**1I** crystal, both supported by C−I···π halogen bonds and N−H^{b}···^{f}O=C hydrogen bonds. For clarity, −CH protons are omitted.

Table S6. Crystallographic data for five selected single crystals of *rac*-**1I** grown in *i*PrOH

No.	1	2	3	4	5
Space group	$P2_12_12_1$	$P2_12_12_1$	$P2_12_12_1$	$P2_12_12_1$	$P2_12_12_1$
a/Å	4.65582(4)	4.65460(10)	4.65380(10)	4.65500(10)	4.65480(10)
b/Å	16.87090(15)	16.8691(2)	16.8730(2)	16.8779(2)	22.9809(6)
c/Å	22.9733(2)	22.9657(3)	22.9596(3)	22.9656(2)	16.8815(4)
α/°	90	90	90	90	90
β/°	90	90	90	90	90
γ/°	90	90	90	90	90
Flack parameter	-0.007(5)	0.022(4)	-0.019(6)	-0.009(13)	0.072(6)
Structure	D-**1I**	D-**1I**	L-**1I**	D-**1I**	L-**1I**

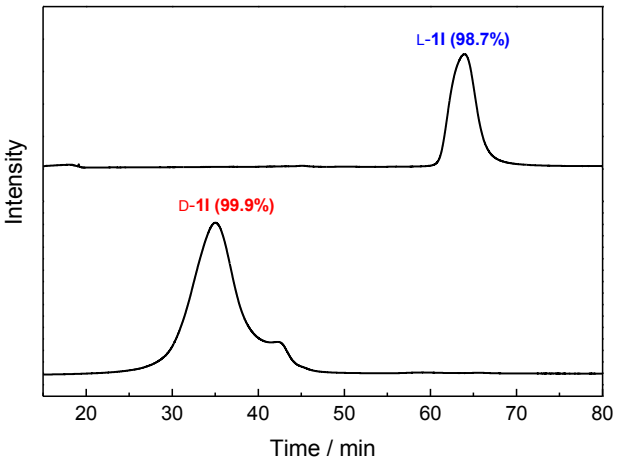

Figure S7. HPLC traces of selected single *rac*-**1I** crystals grown in *i*PrOH. Column: Chiralpak@ID (250 × 4.6 mm). Mobile phase: *n*-hexane/2-propanol = 47:53 (v/v). Flow rate: 1.0 mL/min. Wavelength: UV 270 nm.

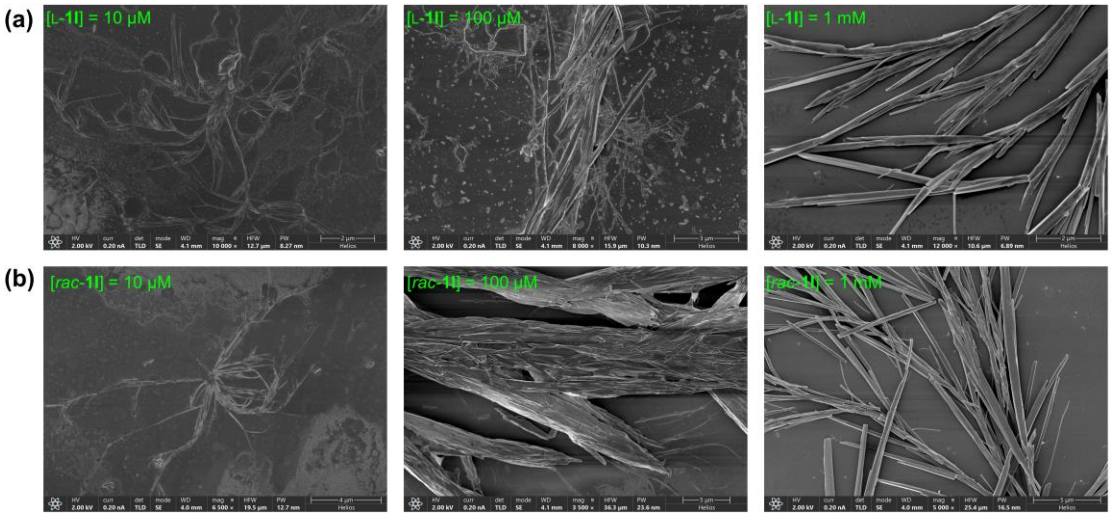

Figure S8. Concentration-dependent SEM images of air-dried samples on platinum-coated silicon wafers of L-**1I** (a) and *rac*-**1I** (b) in *i*PrOH.

Table S7. Crystallographic data for L-**1H**, D-**1H** and *rac*-**1H**

Compound reference	L-**1H** [a]	D-**1H** [a]	*rac*-**1H** [b]
Empirical formula	$C_{17}H_{18}N_4O_2S$	$C_{17}H_{18}N_4O_2S$	$C_{17}H_{18}N_4O_2S$, CH_4O
Formula weight	342.41	342.41	374.45
Temperature/K	100.01(10)	99.9(7)	100.00(10)
Crystal system	orthorhombic	orthorhombic	monoclinic
Space group	$P2_12_12_1$	$P2_12_12_1$	$P2_1/n$
a/Å	4.7117(2)	4.70400(10)	11.7516(2)
b/Å	15.8669(8)	15.8512(3)	8.56240(10)
c/Å	22.3016(12)	22.2569(4)	18.9290(3)
α/°	90	90	90
β/°	90	90	91.2740(10)
γ/°	90	90	90
Volume/Å^3	1667.27(14)	1659.56(6)	1904.20(5)
Z	4	4	4
ρ_{calc}g/cm^3	1.364	1.370	1.306
μ/mm^{-1}	0.212	1.882	1.724
F(000)	720.0	720.0	792.0
Crystal size/mm^3	0.22 × 0.11 × 0.11	0.28 × 0.22 × 0.18	0.20 × 0.16 × 0.12
Radiation	MoKα (λ = 0.71073)	CuKα (λ = 1.54184)	CuKα (λ = 1.54178)
2Θ range for data collection/°	7.308 to 50	6.846 to 153.794	8.77 to 148.608
Index ranges	$-5 \le h \le 4$, $-13 \le k \le 18$, $-17 \le l \le 26$	$-4 \le h \le 5$, $-20 \le k \le 16$, $-25 \le l \le 26$	$-14 \le h \le 13$, $-10 \le k \le 8$, $-21 \le l \le 23$
Reflections collected	4598	6078	11530
Independent reflections	2876 [R_{int} = 0.0223, R_{sigma} = 0.0415]	3069 [R_{int} = 0.0476, R_{sigma} = 0.0559]	3748 [R_{int} = 0.0346, R_{sigma} = 0.0335]
Data/restraints/parameters	2876/0/217	3069/0/218	3748/0/238
Goodness-of-fit on F^2	1.065	1.133	1.057
Final R indexes [I>=2σ (I)]	R_1 = 0.0329, wR_2 = 0.0727	R_1 = 0.0462, wR_2 = 0.1142	R_1 = 0.0381, wR_2 = 0.1019
Final R indexes [all data]	R_1 = 0.0377, wR_2 = 0.0759	R_1 = 0.0536, wR_2 = 0.1388	R_1 = 0.0407, wR_2 = 0.1046
Largest diff. peak/hole / e Å^{-3}	0.31/-0.30	0.71/-0.38	0.29/-0.39
Flack parameter	0.08(5)	0.025(16)	/
CCDC number	1998159	1998160	2068984

[a] Grown in *i*PrOH solution via slow evaporation. [b] Grown in CH_3OH solution via slow evaporation.

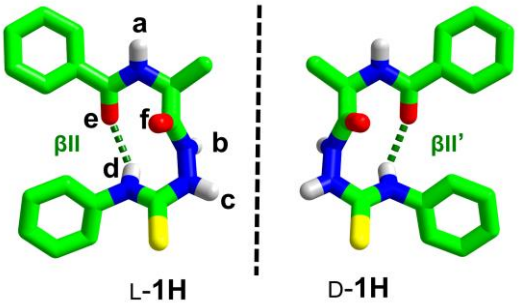

Figure S9. Crystal structures of L-**1H** and D-**1H**, showing βII and βII'-turns, respectively. For clarity, −CH protons are omitted.

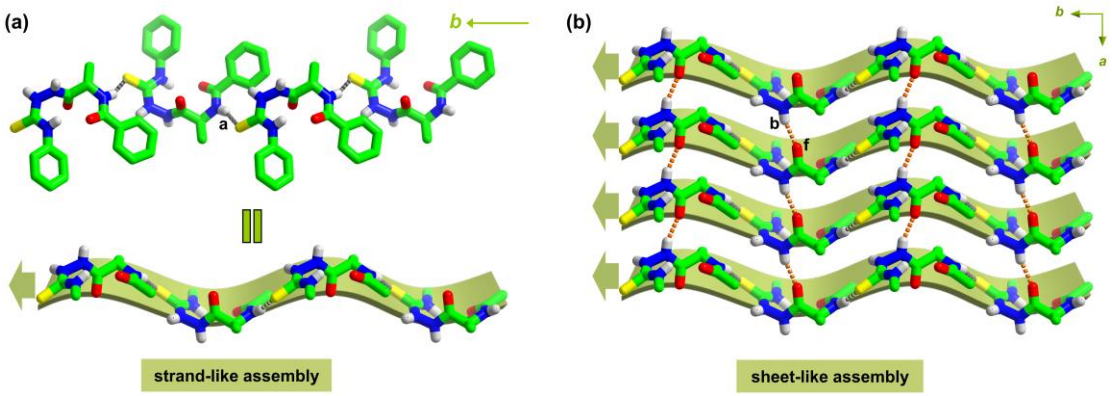

Figure S10. (a) Strand-like 1D assembly from L-**1H** molecules along *b*-axis via intermolecular N−H^{a}···S=C hydrogen bonds (dashed gray lines). (b) N−H^{b}···^{f}O=C hydrogen bonds (dashed orange lines) along *a*-axis link parallel strand-like 1D assemblies into a sheet-like 2D assembly within *ab* plane. For clarity, −CH protons are omitted, in the strand and sheet-like assemblies, phenyl rings are also omitted. The thick arrows indicate the direction of *N*- to *C*-terminus of L-**1H** along the strand structure.

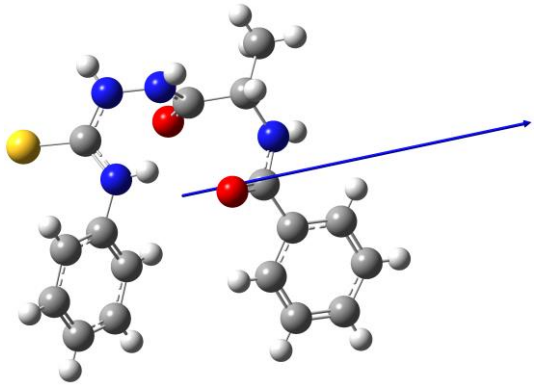

Figure S11. Calculated dipole moment (9.33 D) of L-**1H**, indicating that L-**1H** is polar, which can afford dipole-dipole interactions to the overall van der Waals interactions exhibited in L-**1H** crystal. Method: B3LYP DFT with the 6-311G** basis set.

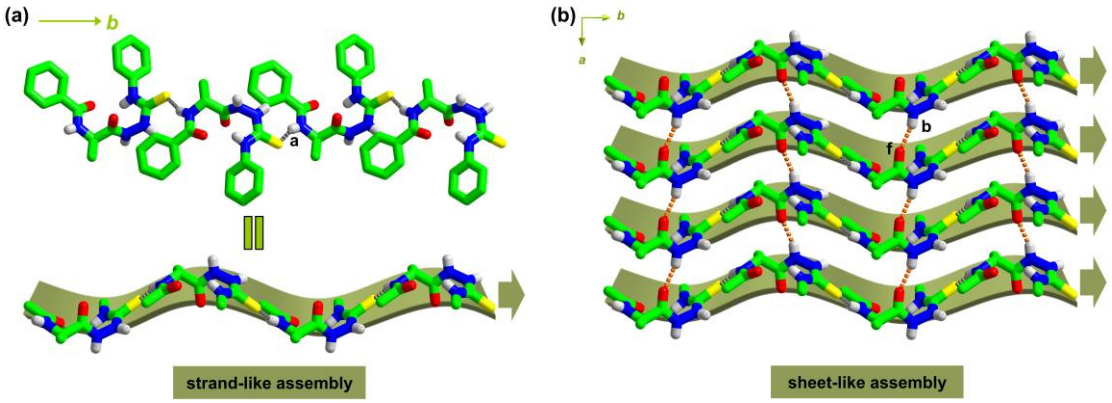

Figure S12. (a) Strand-like 1D assembly from D-**1H** molecules along *b*-axis via intermolecular N−H^{a}···S=C hydrogen bonds (dashed gray lines). (b) N−H^{b}···^{f}O=C hydrogen bonds (dashed orange lines) along the *a*-axis link parallel strand-like 1D assemblies into a sheet-like 2D assembly within *ab* plane. For clarity, −CH protons are omitted, in the strand and sheet-like assemblies, phenyl rings are also omitted. The thick arrows indicate the direction of *N*- to *C*-terminus of D-**1H** along the strand structure.

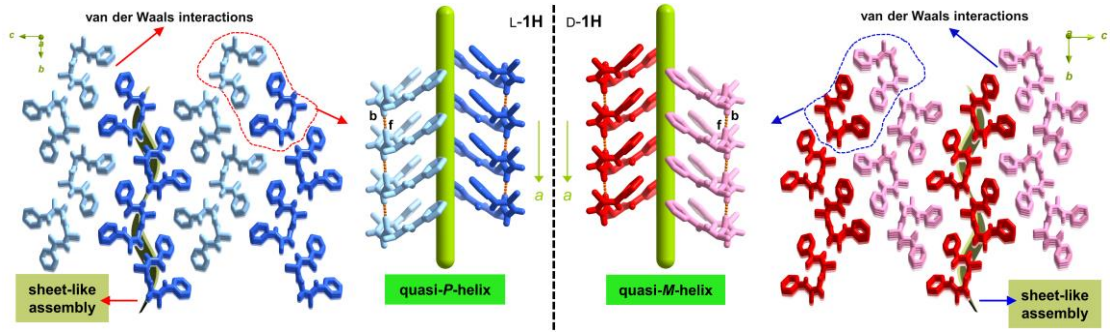

Figure S13. Mirror symmetric 3D superstructures from L-**1H** (left) and D-**1H** (right), consisting of quasi-helical and sheet-like assemblies. While quasi-*P*-helix is formed in L-**1H** crystal, quasi-*M*-helix is formed in D-**1H** crystal, both supported by N−H^{b}···^{f}O=C hydrogen bonds and van der Waals interactions. For clarity, −CH protons are omitted.

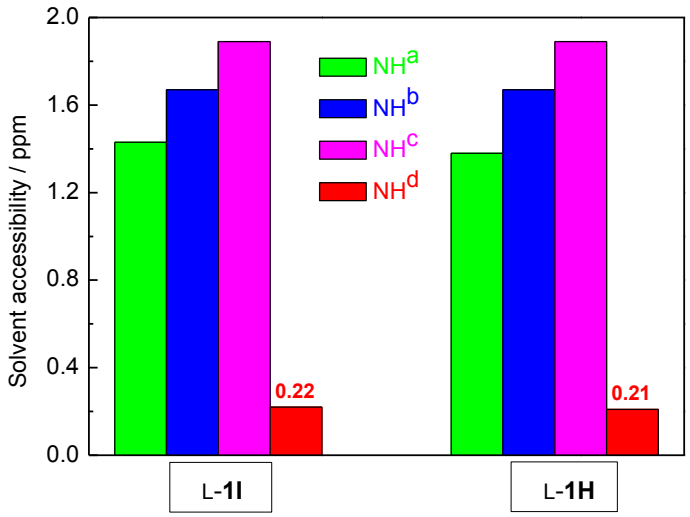

Figure S14. Solvent accessibility of –NH protons in L-**1I** and L-**1H** at 25 °C. Solvent accessibility is given as δ_{NH} in DMSO-d_6 minus δ_{NH} in CD_3CN solutions.[S3] [L-**1I**] = [L-**1H**] = 4 mM. Solvent accessibilities of the thioureido –NH^d protons that are involved in the intramolecular hydrogen bonding are almost the same, suggesting that the strength of β-turn structure in L-**1I** and L-**1H** is comparable in the solution phase.

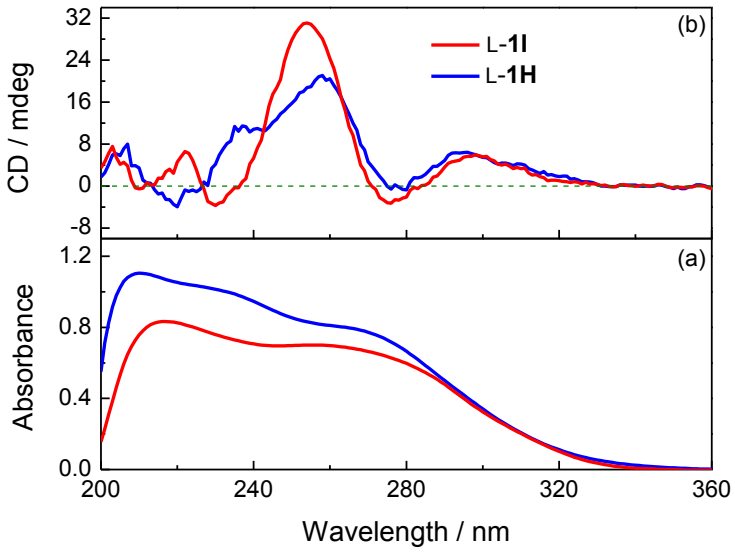

Figure S15. Absorption (a) and CD (b) spectra of L-**1I** and L-**1H** crystals.

Table S8. Crystallographic data for five single crystals of *rac*-**1H** grown in *i*PrOH

No.	1	2	3	4	5
Space group	$P2_12_12_1$	$P2_12_12_1$	$P2_12_12_1$	$P2_12_12_1$	$P2_12_12_1$
a/Å	4.69890(10)	4.70300(10)	4.69510(10)	4.69330(10)	4.69942(4)
b/Å	15.8791(4)	15.8556(2)	15.8762(3)	15.8695(4)	15.85612(15)
c/Å	22.2710(6)	22.2560(3)	22.2731(5)	22.2403(5)	22.24912(19)
α/°	90	90	90	90	90
β/°	90	90	90	90	90
γ/°	90	90	90	90	90
Flack parameter	-0.485(9)	0.350(7)	-0.478(12)	-0.440(10)	-0.194(5)
Structure	L-**1H**	L-**1H**	D-**1H**	L-**1H**	L-**1H**

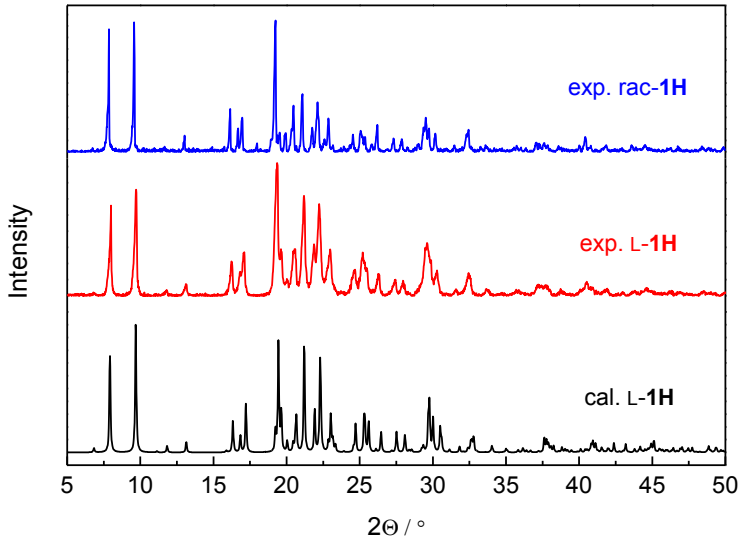

Figure S16. Calculated and experimental XRPD patterns of L-**1H** crystals and experimental XRPD of *rac*-**1H** crystals grown in *i*PrOH. The identical XRPDs of L-**1H** and *rac*-**1H** crystals indicate that *rac*-**1H** forms racemic conglomerates in *i*PrOH.

Table S9. Determined *ee* values for five selected single crystals of *rac*-**1H** grown in *i*PrOH[a]

No.	1	2	3	4	5
ee	9.2%	-58%	8.6%	-4.8%	2.0%

[a] Column: Chiralpak@ID (250 × 4.6 mm). Mobile phase: *n*-hexane/2-propanol = 47:53 (v/v). Flow rate: 1.0 mL/min. Wavelength: UV 270 nm.

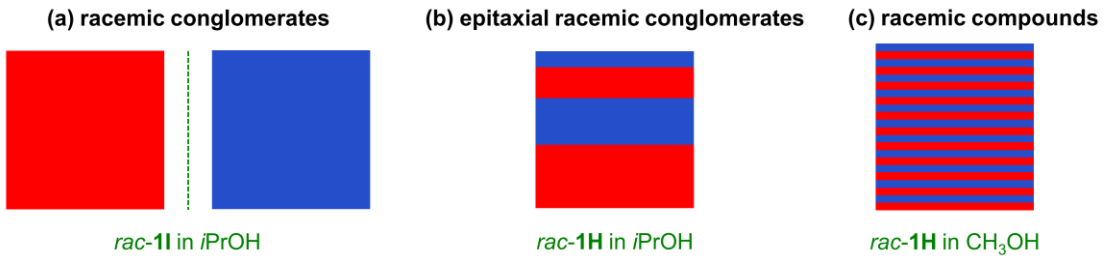

Figure S17. Schematic representation of racemic conglomerates formed from *rac*-**1I** in *i*PrOH (a), epitaxial racemic conglomerates formed from *rac*-**1H** in *i*PrOH (b),[S4,S5] and racemic compounds formed from *rac*-**1H** in CH_3OH.

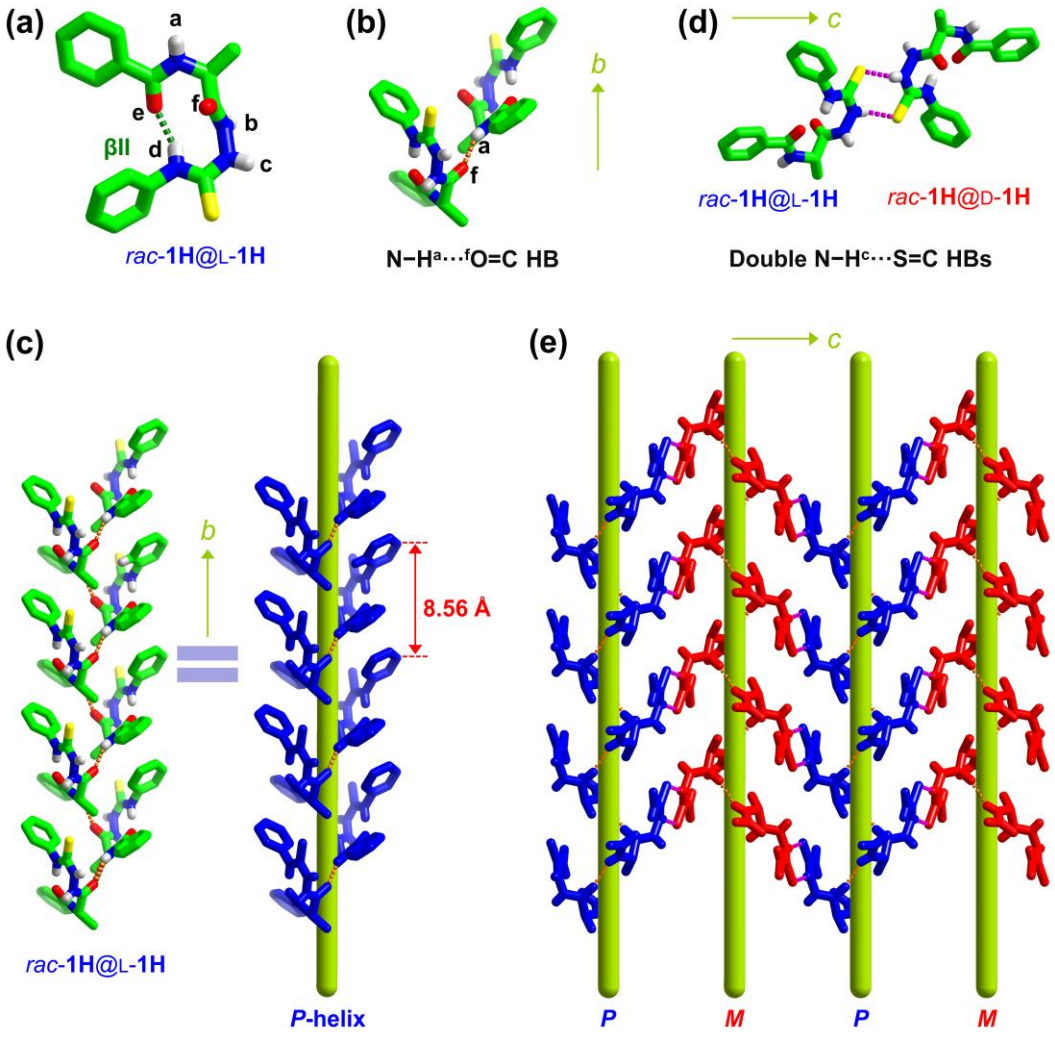

Figure S18. 2D Supramolecular structure in the *bc* plane of *rac*-**1H** crystal grown in CH_3OH. (a) Crystal structure of *rac*-**1H**@L-**1H**, showing a βII-turn. (b) N−H^{a}···^{f}O=C hydrogen bond (HB, dashed orange line) between adjacent *rac*-**1H**@L-**1H** molecules along the *b*-axis. (c) Supramolecular *P*-helix from *rac*-**1H**@L-**1H** molecules along the *b*-axis via N−H^{a}···^{f}O=C hydrogen bonds (dashed orange lines). (d) Double N−H^{c}···S=C hydrogen bonds (dashed pink lines)

between adjacent *rac*-**1H**@L-**1H** and *rac*-**1H**@D-**1H** molecules along the *c*-axis. (e) 2D superstructure of alternative *P*- and *M*-helices linked by double N−H^{c}···S=C hydrogen bonds (dashed pink lines). For clarity, all −CH protons are omitted. In (e), *rac*-**1H**@L-**1H** molecules are depicted in blue, while *rac*-**1H**@D-**1H** molecules are depicted in red, phenyl rings are omitted for clarity.

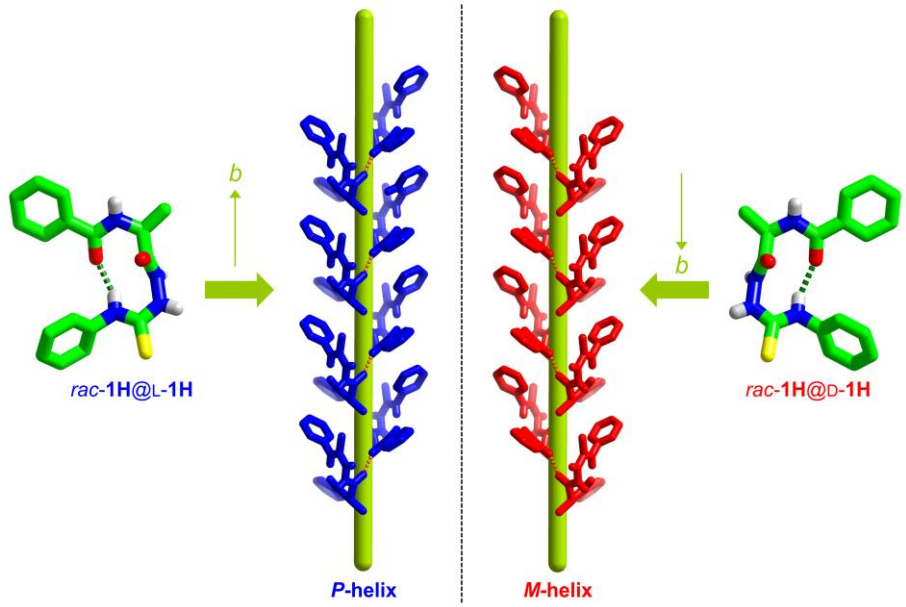

Figure S19. Supramolecular *P*-helix formed from *rac*-**1H**@L-**1H** (left) and *M*-helix formed from *rac*-**1H**@D-**1H** (right) along the *b*-axis in *rac*-**1H** crystal that grown in CH_3OH. For clarity, −CH protons are omitted.

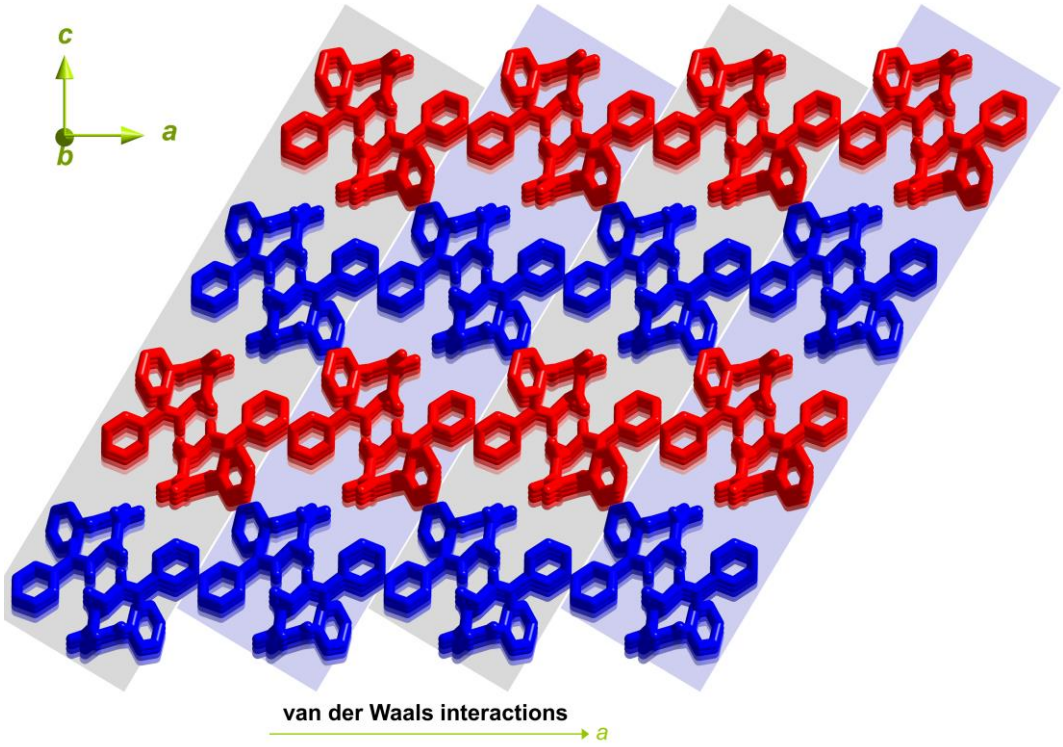

Figure S20. X-ray 3D superstructure of *rac*-**1H** crystal that grown in CH_3OH. The heterochiral *bc* planes stack via van der Waals interactions in parallel manner along the *a*-axis. For clarity, −CH protons are omitted.

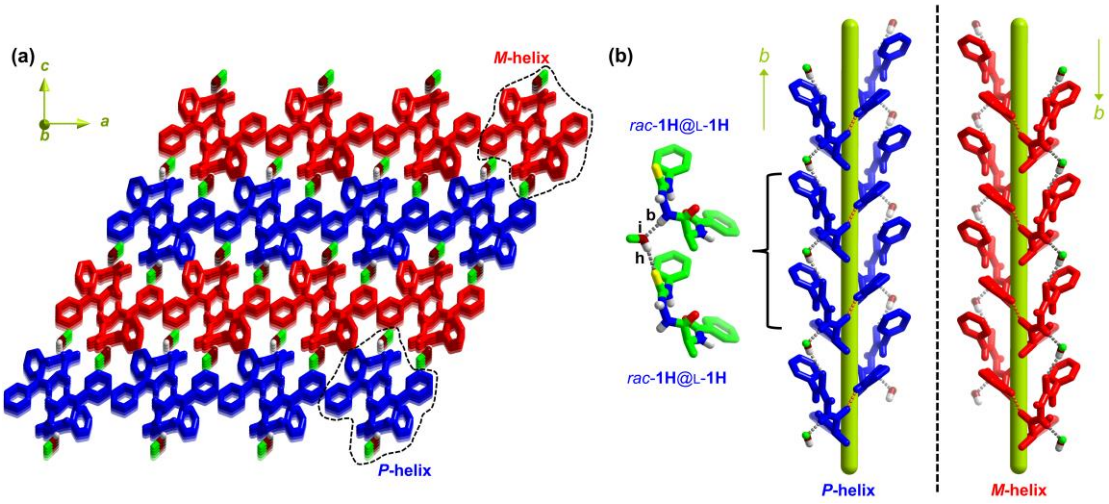

Figure S21. (a) Embedment of solvent CH_3OH molecules in *rac*-**1H** crystal. (b) Along the *b*-axis, solvent CH_3OH molecules afford intermolecular hydrogen bonds ($^{i}O{-}H^{h}\cdots S{=}C$ and $N{-}H^{b}\cdots{}^{i}O{-}H^{h}$ hydrogen bonds) to stabilize the supramolecular *P*-helix from *rac*-**1H**@L-**1H** and *M*-helix from *rac*-**1H**@D-**1H**. For clarity, −CH protons are omitted.

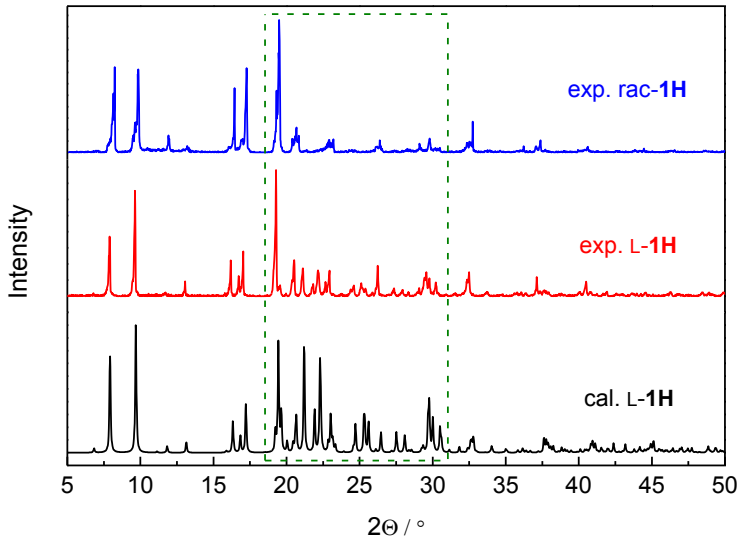

Figure S22. Calculated and experimental XRPD patterns of L-**1H** crystals and experimental XRPD of *rac*-**1H** crystals grown in CH_3OH. The different XRPDs of L-**1H** and *rac*-**1H** crystals indicate that *rac*-**1H** forms racemic compounds in CH_3OH.

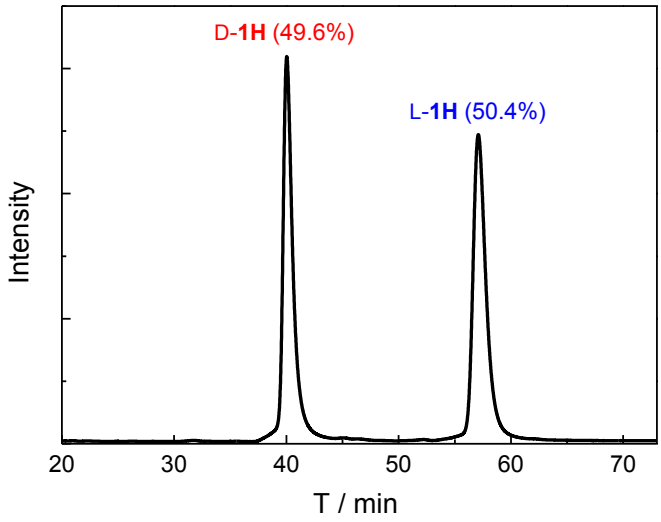

Figure S23. HPLC traces of one single *rac*-**1H** crystal grown in CH_3OH. Column: Chiralpak@ID (250 × 4.6 mm). Mobile phase: *n*-hexane/2-propanol = 47:53 (v/v). Flow rate: 1.0 mL/min. Wavelength: UV 270 nm.

3. ^{1}H NMR and ^{13}C NMR spectra

^{1}H NMR of L-**1I** (500 MHz, DMSO-d_6)

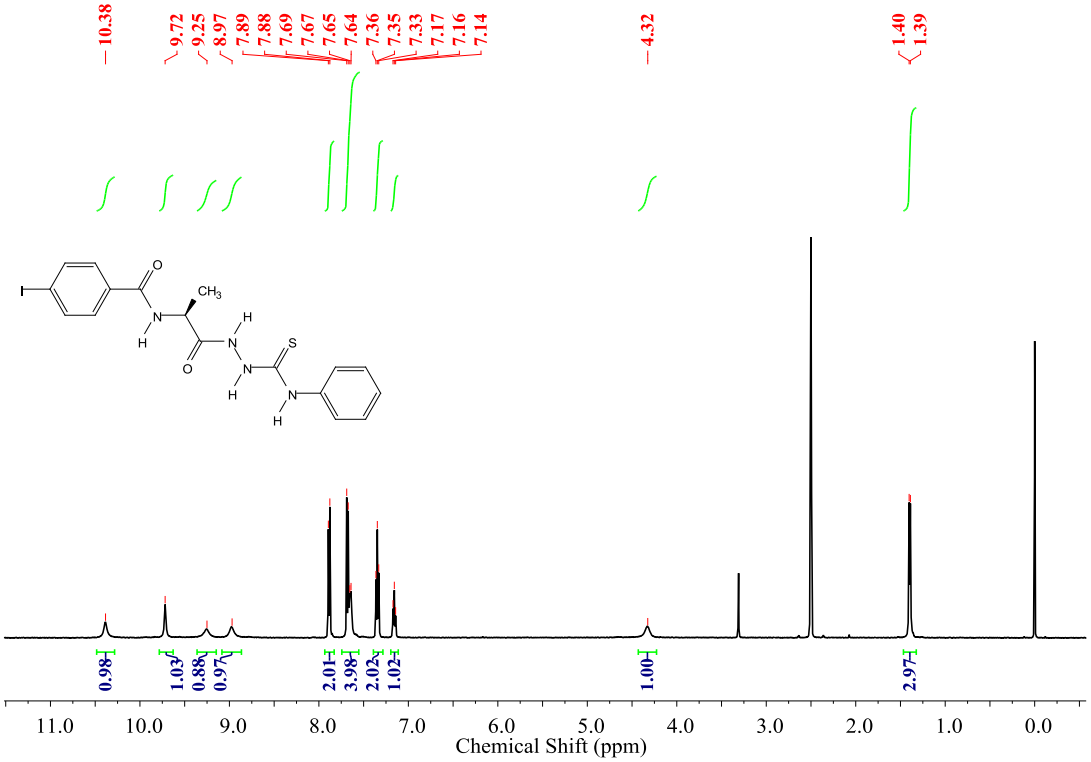

^{13}C NMR of L-**1I** (151 MHz, DMSO-d_6)

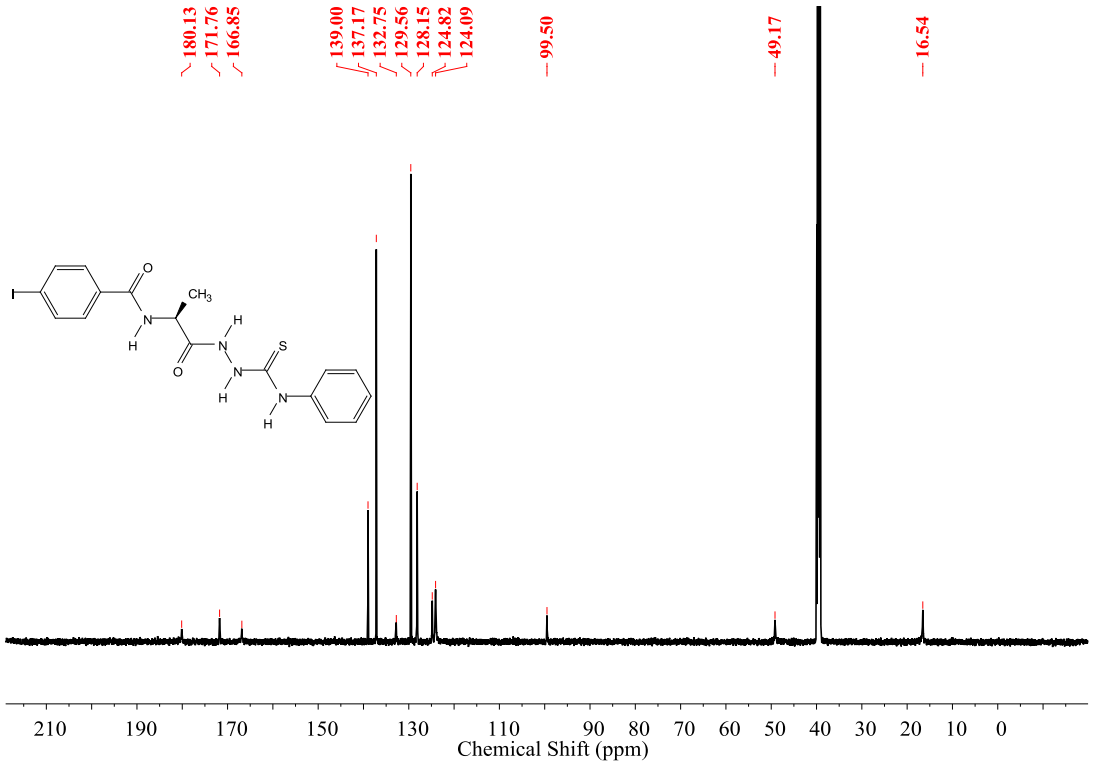

^{1}H NMR of D-**1I** (500 MHz, DMSO-d_6)

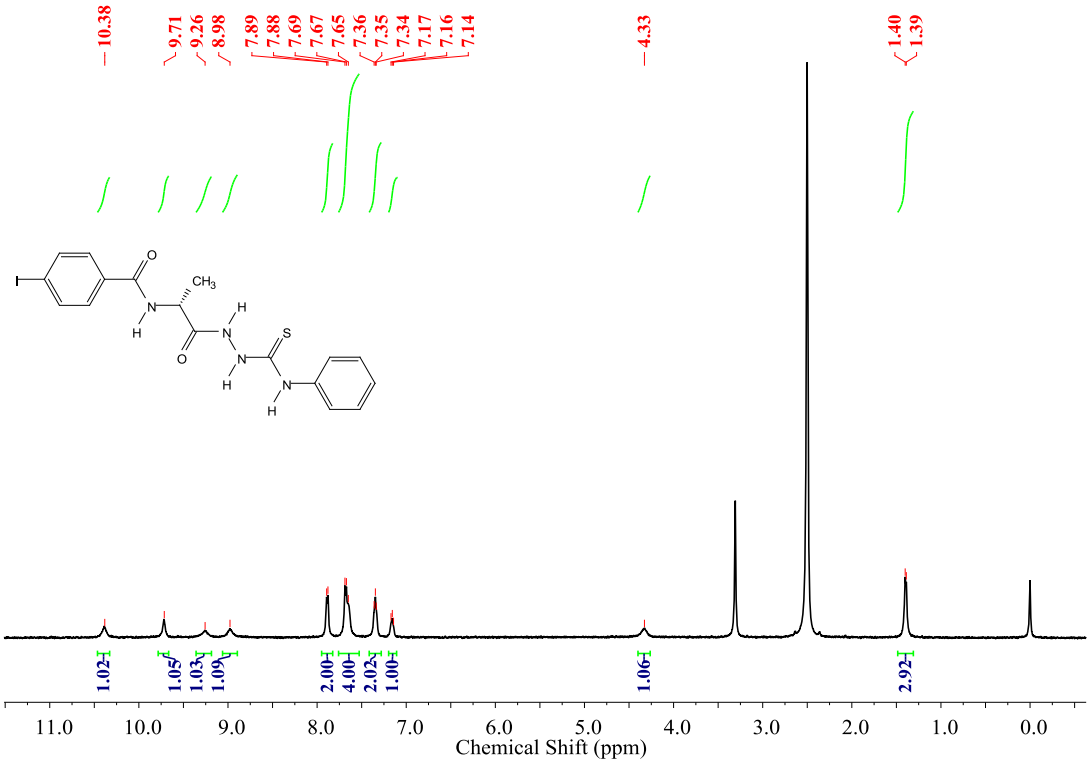

^{13}C NMR of D-**1I** (151 MHz, DMSO-d_6)

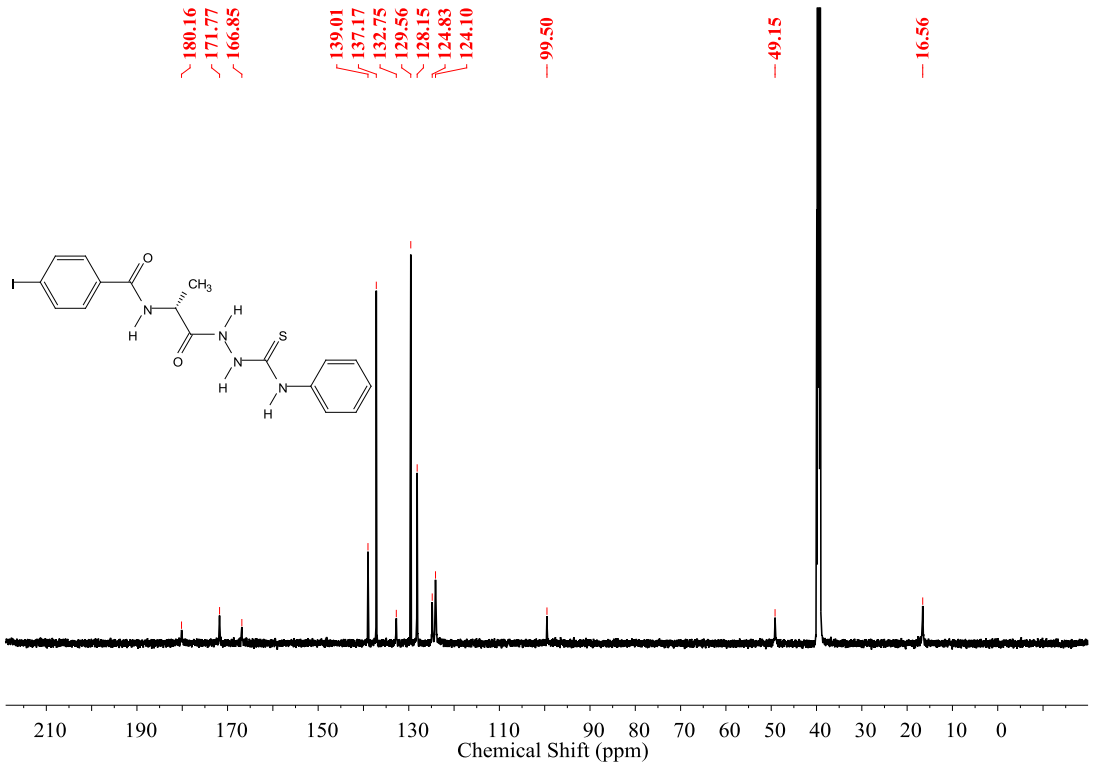

^{1}H NMR of L-**1H** (500 MHz, DMSO-d_6)

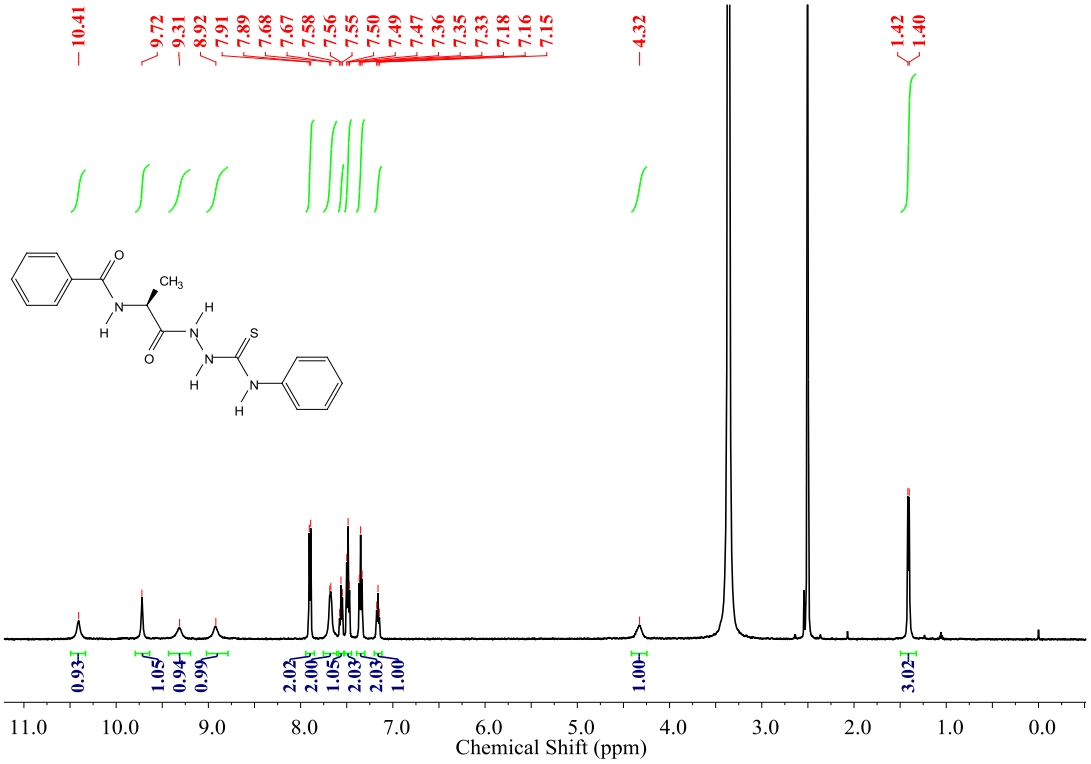

^{13}C NMR of L-**1H** (214 MHz, CD_3CN)

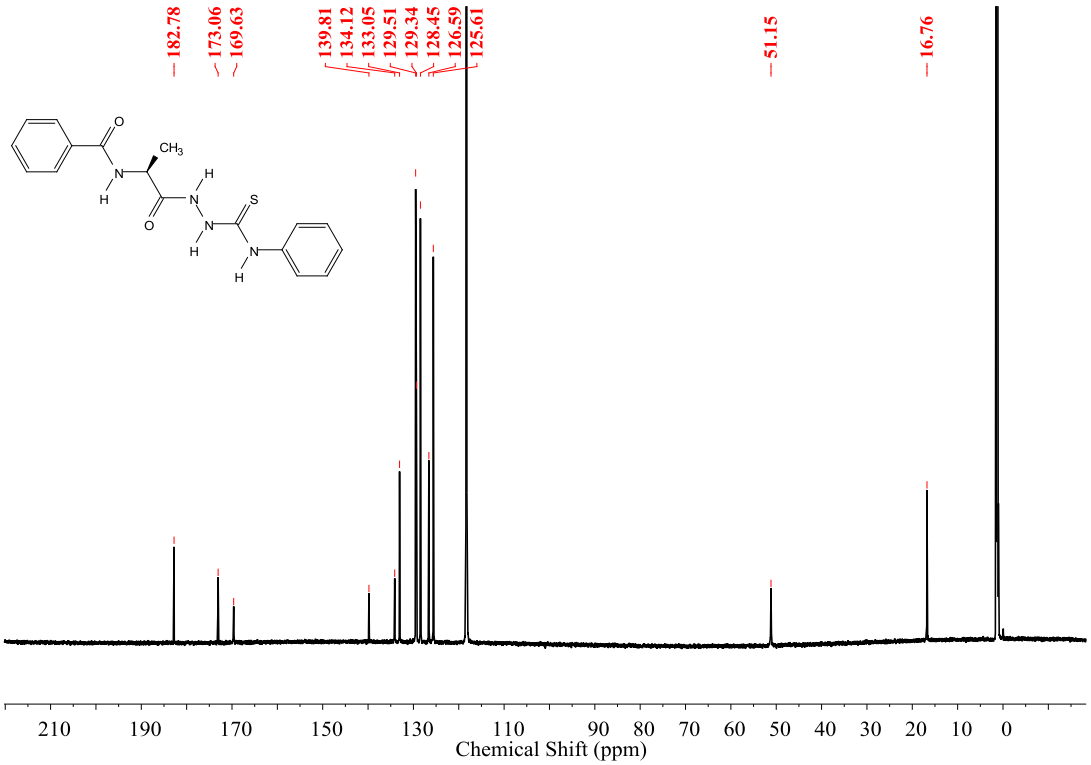

^{1}H NMR of D-**1H** (500 MHz, DMSO-d_6)

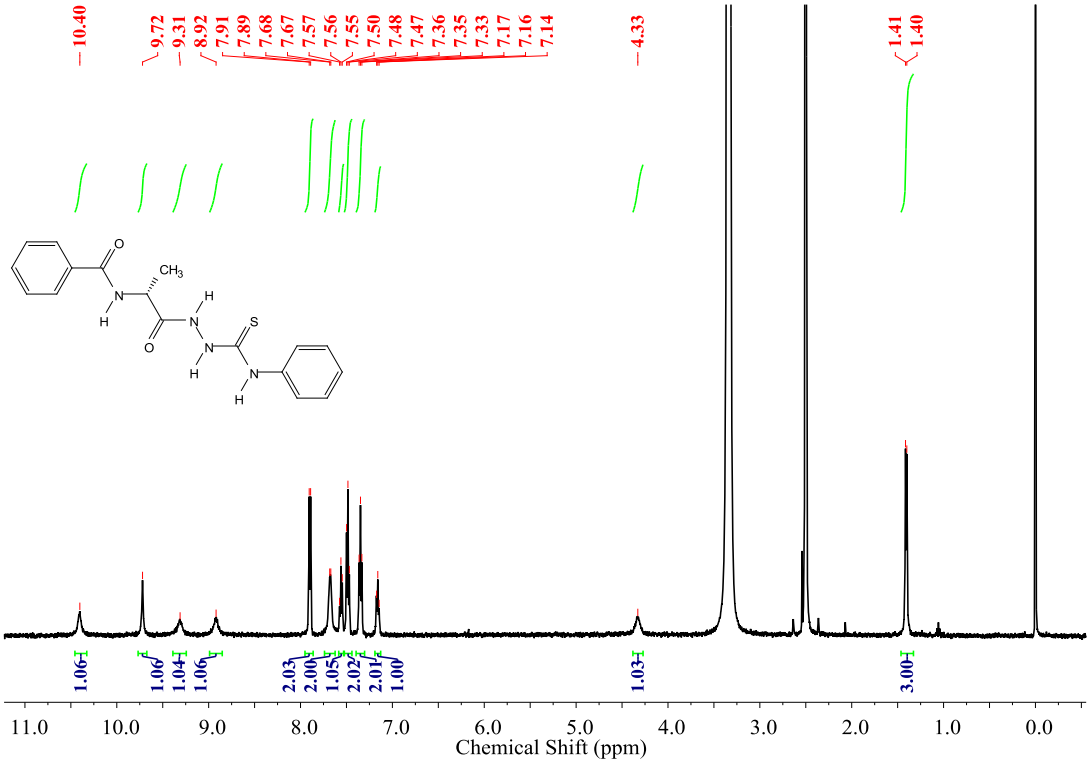

^{13}C NMR of D-**1H** (214 MHz, CD_3CN)

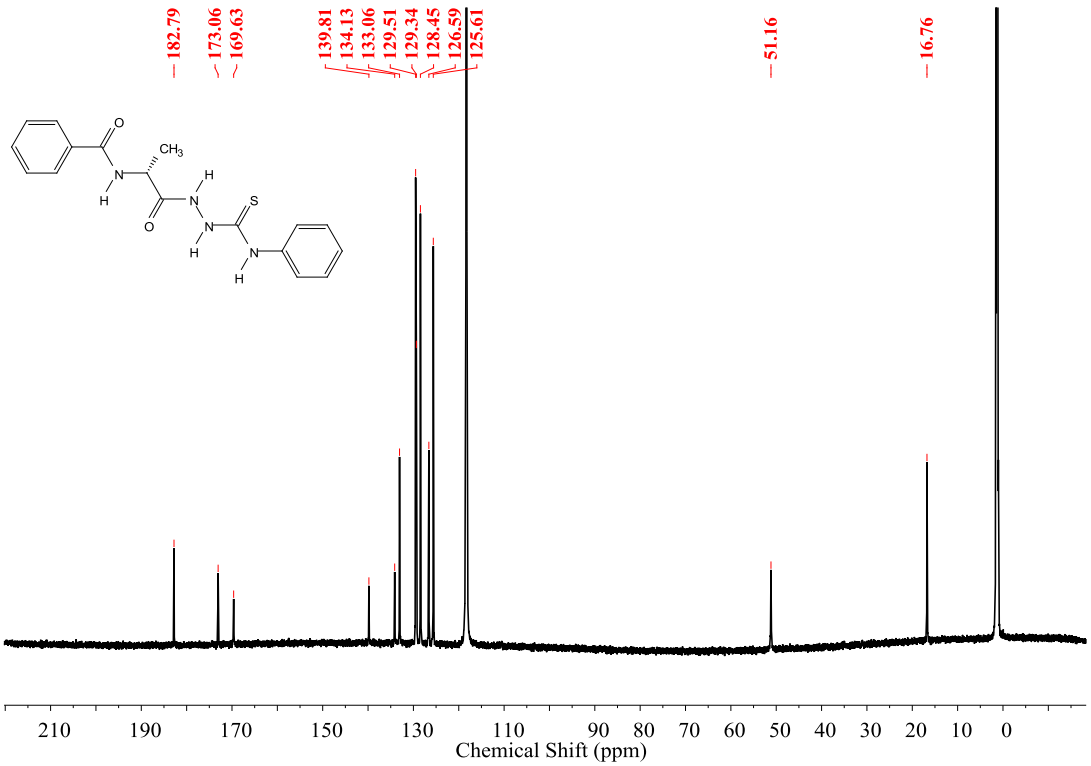

^{1}H NMR of L-**2I** (500 MHz, DMSO-d_6)

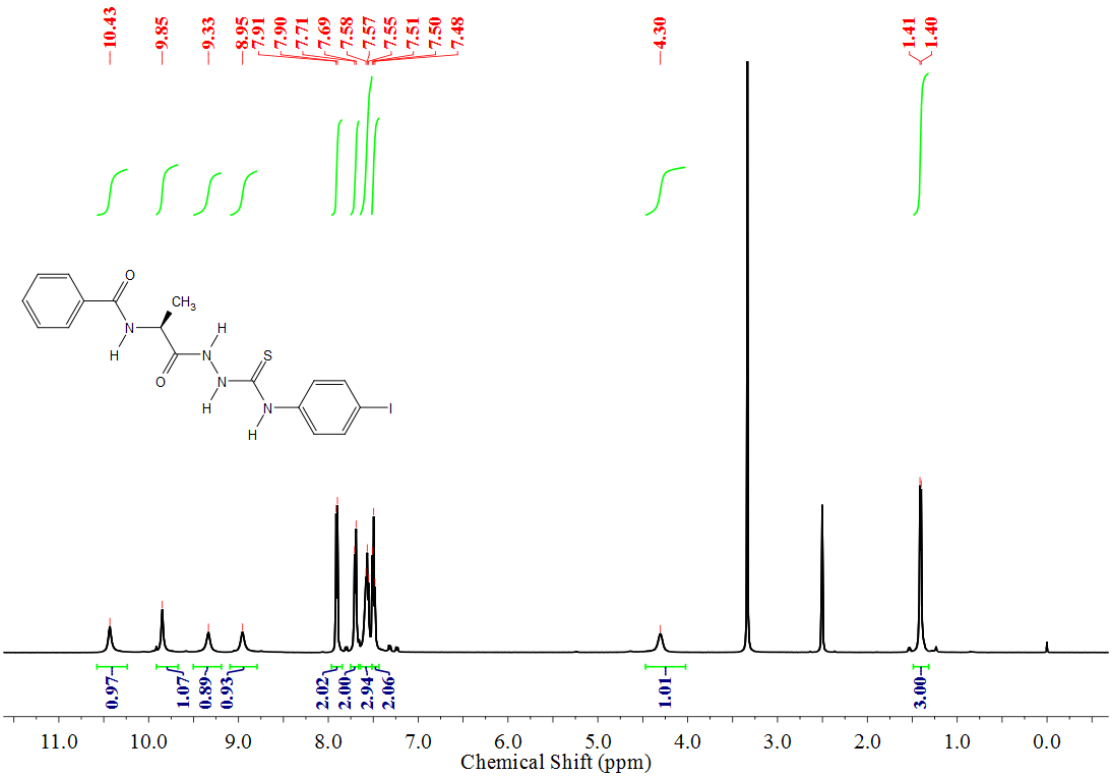

^{13}C NMR of L-**2I** (214 MHz, DMSO-d_6)

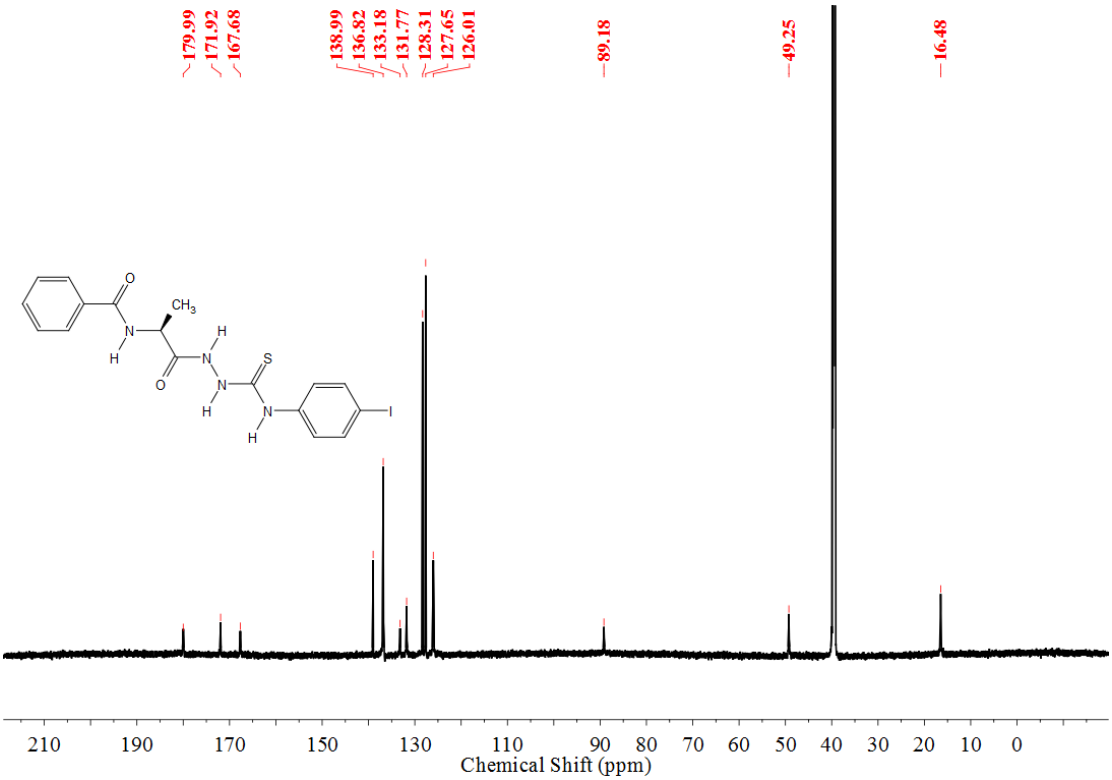

^{1}H NMR of D-**2I** (500 MHz, DMSO-d_6)

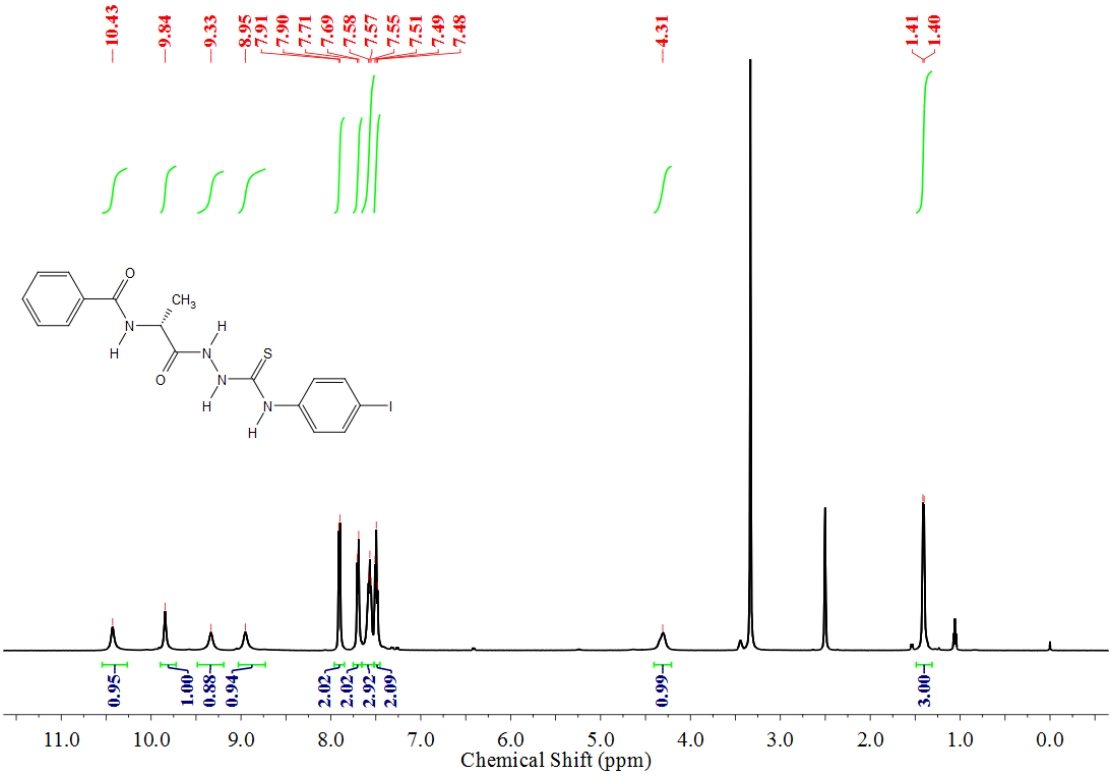

^{13}C NMR of D-**2I** (214 MHz, DMSO-d_6)

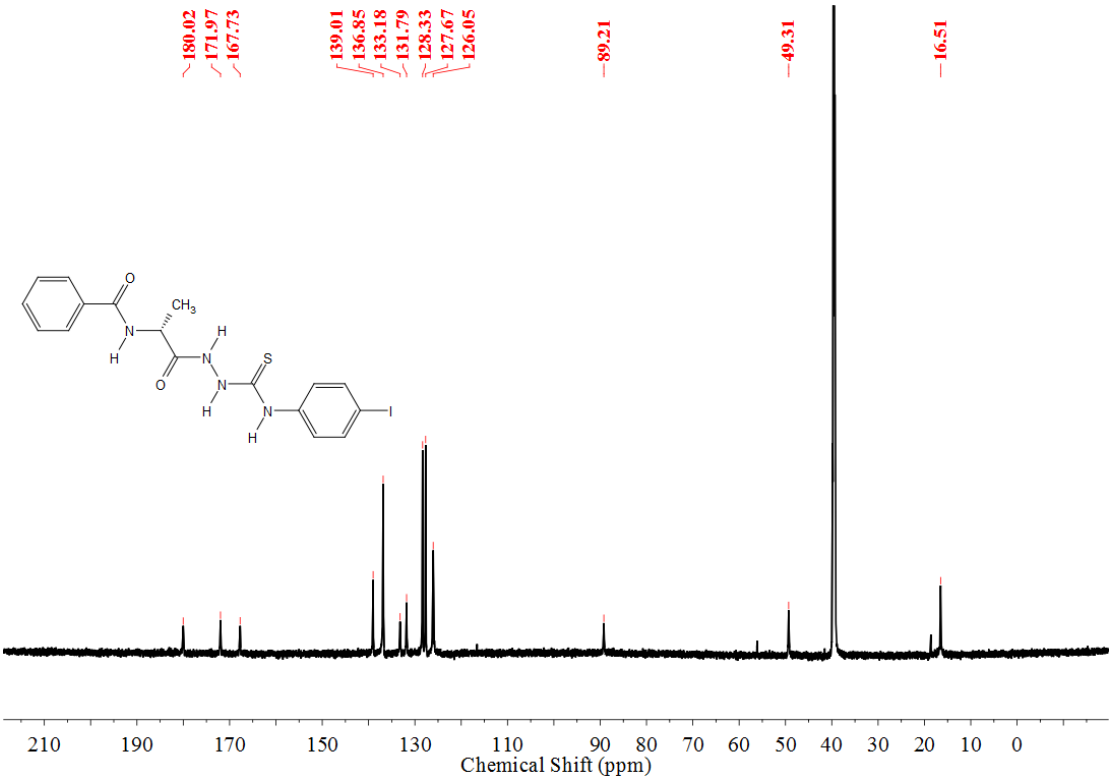

^{1}H NMR of L-**3I** (500 MHz, DMSO-d_6)

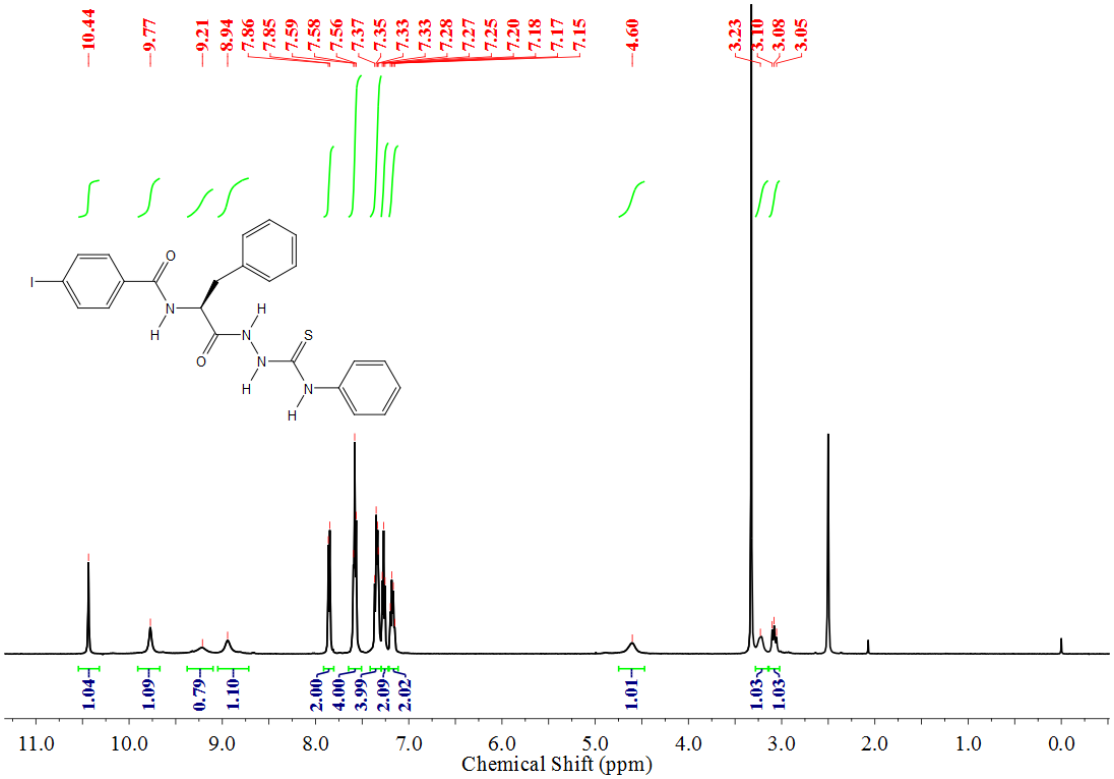

^{13}C NMR of L-**3I** (151 MHz, DMSO-d_6)

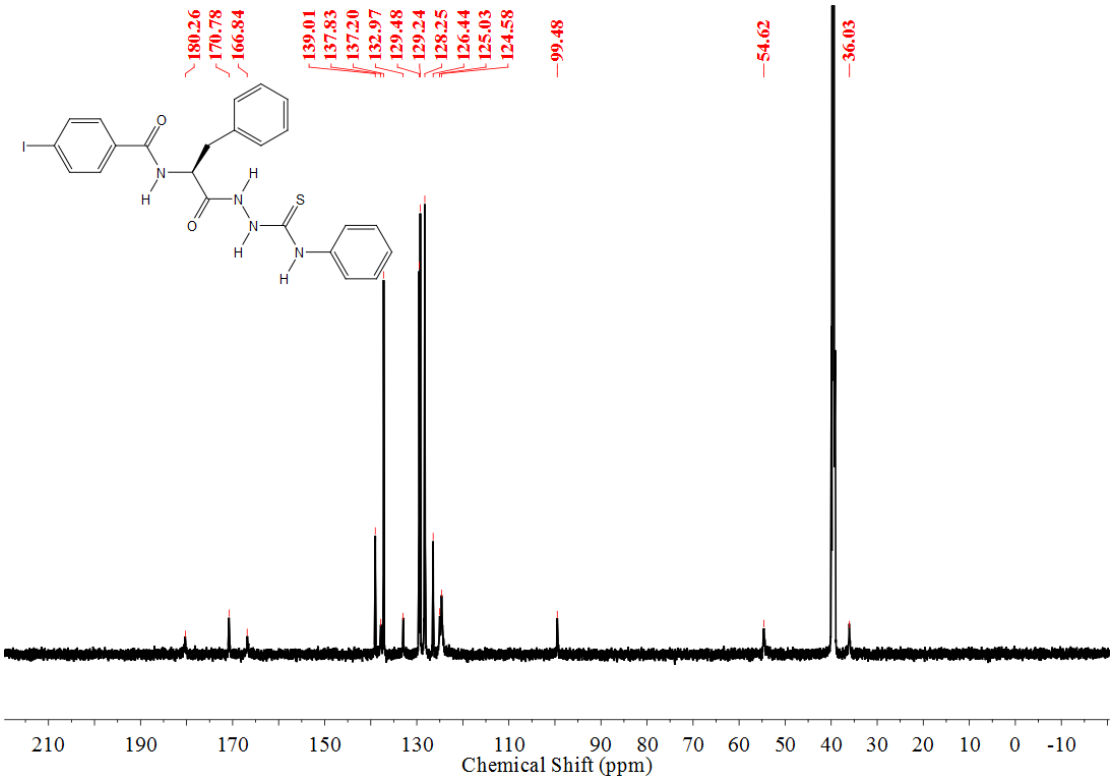

^{1}H NMR of D-**3I** (600 MHz, DMSO-d_6)

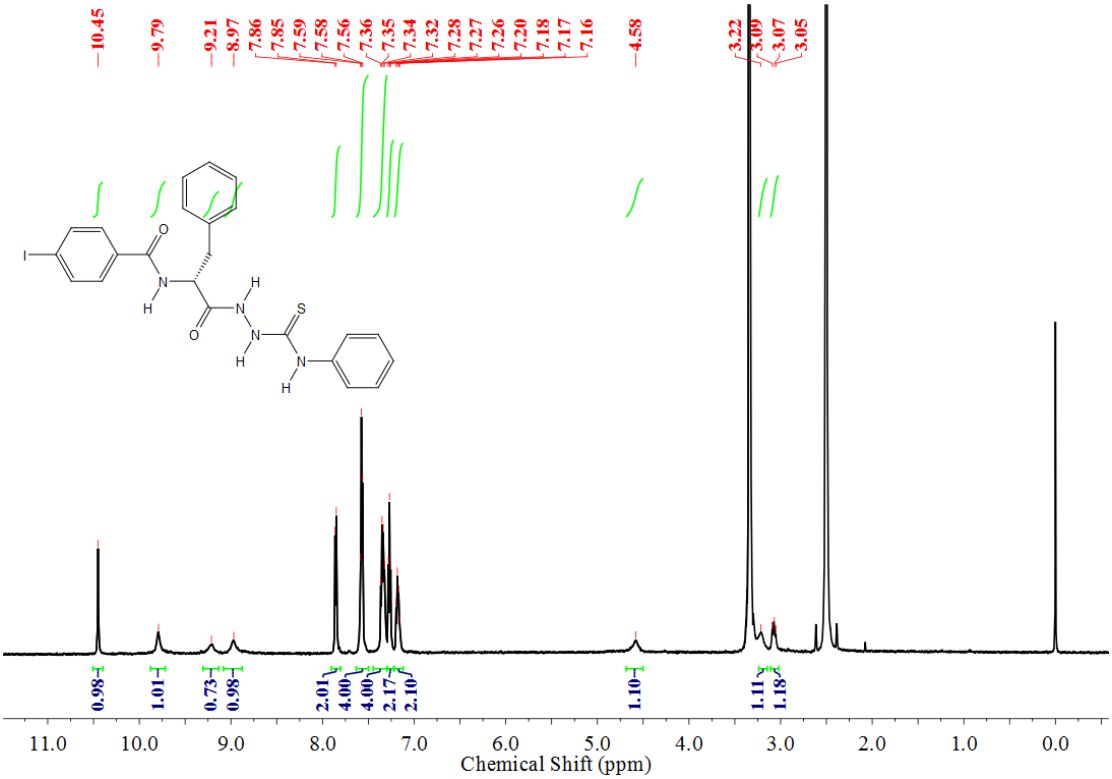

^{13}C NMR of D-**3I** (126 MHz, DMSO-d_6)

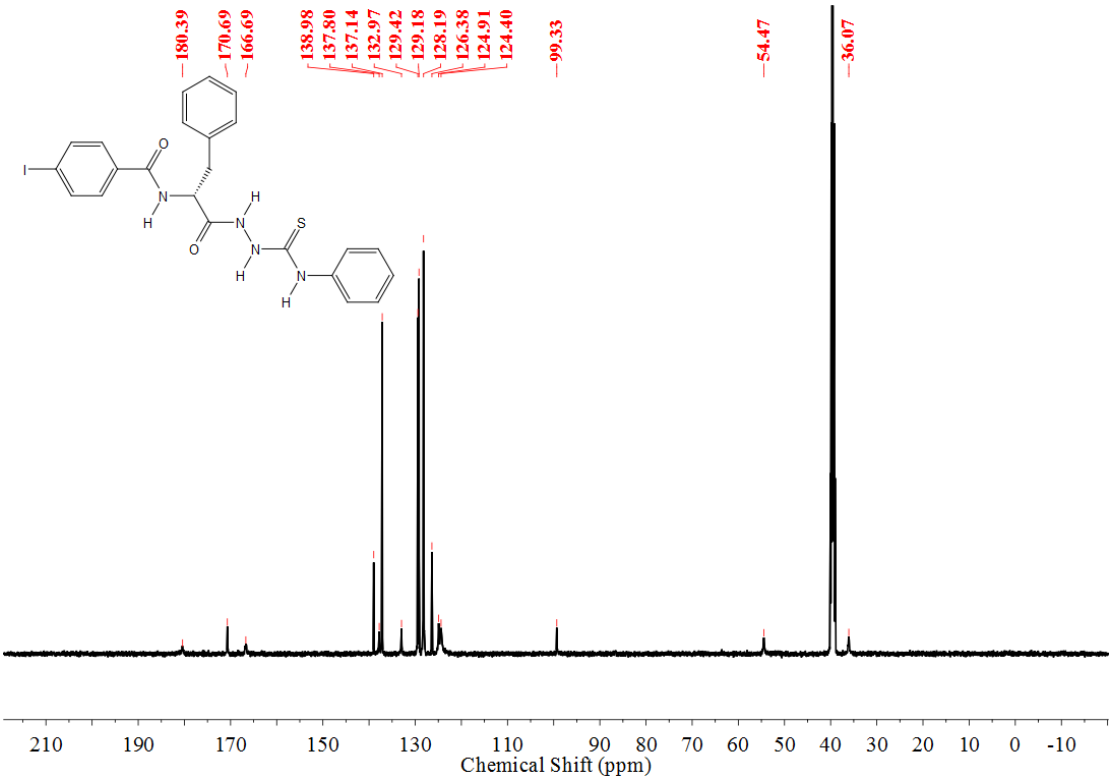

4. References

S1. Yan, X.; Zou, K.; Cao, J.; Li, X.; Zhao, Z.; Li, Z.; Wu, A.; Liang, W.; Mo, Y.; Jiang, Y. Single-handed supramolecular double helix of homochiral bis(*N*-amidothiourea) supported by double crossed C−I···S halogen bonds. *Nat. Commun.* **2019**, *10*, 3610.

S2. Koch, O. Advances in the Prediction of Turn Structures in Peptides and Proteins. *Mol. Inf.* **2012**, *31*, 624-630.

S3. Copeland, G. T.; Jarvo, E. R.; Miller, S. J. Minimal Acylase-Like Peptides. Conformational Control of Absolute Stereospecificity. *J. Org. Chem.* **1998**, *63*, 6784-6785.

S4. van Enckevort, W. J. P. On the Crystallization of Epitaxial Racemic Conglomerates. *J. Phys. Chem. C* **2010**, *114*, 21593-21604.

S5. Spix, L.; Alfring, A.; Meekes, H.; van Enckevort, W. J. P.; Vlieg, E., Formation of a Salt Enables Complete Deracemization of a Racemic Compound through Viedma Ripening. *Cryst. Growth Des.* **2014**, *14*, 1744-1748.